Subcontractor Report

Process Development for CIGS Based Thin Film Photovoltaic Modules

Final Technical Report
5 February 1998–4 February 2001

J. Britt, S. Wiedeman, M. Beck, and S. Albright
Global Solar Energy, Inc.
Tucson, Arizona

NREL

National Renewable Energy Laboratory

Process Development for CIGS Based Thin Film Photovoltaic Modules

Final Technical Report
5 February 1998–4 February 2001

J. Britt, S. Wiedeman, M. Beck, and S. Albright
Global Solar Energy, Inc.
Tucson, Arizona

NREL

National Renewable Energy Laboratory

NOTICE

Table of Contents

List of Figures

List of Tables

Abstract

As a technology partner with NREL, Global Solar Energy (GSE) initiated an extensive and systematic plan to accelerate the commercialization of thin film photovoltaics (PV) based on Copper Indium Gallium diSelenide (CIGS). The distinguishing feature of the GSE manufacturing process is the exclusive use of lightweight, flexible substrates. GSE developed the technology to fabricate CIGS photovoltaics on both stainless steel and polymer substrates; over the course of the TFPP program, however, stainless steel showed significant advantages. CIGS deposited on flexible substrates can be fabricated into either flexible or rigid modules. Low-cost, rigid PV panels for remote power, bulk/utility, telecommunication, and rooftop applications have been produced by affixing the flexible substrate to an inexpensive rigid panel by lamination or adhesive.

In the GSE approach, continuous rolls of substrate as long as 1000 feet are processed, as opposed to individual small glass plates. Stainless steel based PV modules are fabricated by a novel interconnect method that avoids the use of wires or foils and soldered connections. In the case of polymer based PV modules, the continuous roll is not sectioned into individual panels until the module buss and power leads are attached. Roll-to-roll vacuum deposition has several advantages that translate directly into reduced capital costs, greater productivity, improved yield, greater reliability, lower maintenance, and a larger volume of PV material.

In combination with roll-to-roll processing, GSE has developed evaporation deposition operations that enable low-cost and high-efficiency CIGS modules. In-line multi-source evaporation has been demonstrated at GSE to allow production of high-quality CIGS films in a continuous roll-to-roll operation. Multi-source evaporation has other advantages including direct absorber formation (no selenization heat treatment) and high materials utilization of low-cost feed stock.

The CIGS deposition process relies heavily on effusion source technology developed at GSE, and solving numerous problems was an integral part of the source development effort. At present, the robust effusion sources are capable of depositing high-quality coatings over large areas. Significant challenges still exist for increasing the source capacity to enable even longer depositions and improving the control of effusion rate during production runs.

CIGS process development has been focused on synchronizing the operation of the effusion sources, delivery profile, substrate temperature, and a host of other parameters. The primary vehicle for CIGS process development in Phase III was a 12-inch production system. Thin film coating process development was conducted primarily on stainless steel foil during Phase III to allow issues of monolithic integration and coating processes to be separated.

Development of techniques for monolithic integration was performed on polyimide substrate. Cell interconnection for thin film CIGS modules on a polyimide substrate presents a considerable challenge. Substantial progress has been made in the development of all-laser processes for monolithic integration. The interconnect scheme requires both an ink-jet deposition step and the removal of material by selective laser scribing. All laser scribes have been demonstrated and optimized to minimize electrical losses. Continuous ink-jet lines less than 200μm in width are routinely achieved, a noticeable advantage over screen-printing.

In the area of new product development and demonstration, progress has been made in several fields. Unlaminated submodules on a rigid substrate for use as rooftop shingles have been developed with a strategic business partner. Modules utilizing a reinforced nylon backing are the basis for two GSE product lines with attributes of light weight, durability, and portability. Modules that utilize a semi-rigid, thin aluminum backing for added strength in the field and for a standard UL rate-able product line have been demonstrated. The semi-rigid module designs have been submitted to UL and a contract for UL testing is in place. Critical product certification equipment has been procured and validated at the GSE Tucson facility to accelerate the required testing. Products have been demonstrated in selected market sectors for early feedback from customers.

INTRODUCTION

Thin film photovoltaic (PV) modules are the next evolutionary step towards cost-effective generation of electricity from sunlight. Thin film Copper Indium Gallium diSelenide (CIGS) has been established as a leading contender to achieve that goal. Global Solar Energy (GSE) was founded to capitalize on the natural advantages of CIGS and develop a cost-efficient manufacturing scheme to bring the technology to market in a user-friendly form. The heart of the manufacturing scheme is all roll-to-roll vacuum processing on a continuous flexible substrate; this was initially conceived to be polyimide, but over the course of the TFPP program, stainless steel has shown significant advantages.

There have been numerous challenges in developing the technology for manufacturing flexible CIGS photovoltaic modules. Three major areas deemed exceptionally challenging were selected by GSE for focused development under the Thin Film Partnership Program: 1) CIGS absorber improvement, 2) monolithic integration, and 3) encapsulation. Most conventional techniques for monolithic integration of thin film PV devices on glass substrates cannot be applied to integrate devices on a polyimide substrate. Novel interconnect schemes and processes had to be developed. The encapsulation of a flexible module also presented special problems to solve, and unique advantages to employ.

In Phase I, the primary issues addressed to improve the CIGS absorber were control of effusion sources and development of processes that would yield high-quality CIGS thin films. In particular, scaling up the source design for multi-source co-evaporation over large areas (33 cm × 300 meter rolls of substrate) with adequate uniformity was an important goal. During this phase, a complete set of effusion sources was successfully demonstrated, as was a 9.8% device from CIGS deposited on polyimide in a roll-coater. Other accomplishments included: continual verification of process compatibility with CdS and TCO depositions; initiation of a program to incorporate Na into roll-coated CIGS films, and initial exploration of roll-to-roll CIGS deposition on stainless steel – with demonstration of an 8.4% efficient device.

Electrical and microscopic techniques were used to verify many aspects of the back contact, via, and front contact scribes, and continuous ink lines less than 200 μm wide were demonstrated with the ink dispense technology – an integral part of the interconnect scheme. Also, equipment to accomplish rapid lamination throughput of product at low cost for all initially envisioned product lines was identified, two laminators were installed, and laminated active modules were demonstrated. Finally, first-generation methods for lead termination (buss bar to lead connection) were incorporated into the "standard" process, and a conceptual design for a "buss bar and lay-up apparatus" was completed.

In Phase II, the primary issues addressed to improve the CIGS absorber remained the same. Significant improvements to the effusion source design and operation were made, allowing deposition of high quality coatings over large areas. Remaining challenges included increasing source capacity to enable even longer depositions and improving control of effusion rate during production runs.

A milestone achievement during this phase was demonstration of an 11.5% device from CIGS deposited on stainless steel web. Also, process improvement tests validated the beneficial effects of Na doping, which was subsequently implemented in the production equipment, and ongoing verification of GSE process compatibility with CdS and TCO depositions continued.

Other accomplishments included: substantial improvement of the monolithic integration of PV cells on polyimide substrate; electrical and microscopic verification of most aspects of the back contact, via, and front contact scribes, and exceptional reproducibility of continuous ink lines less than 200 μm wide produced with ink dispense technology. In the new product area, modules that utilize a reinforced nylon backing and provide support for two lightweight, durable, and portable GSE product lines were developed, and modules that utilize a semi-rigid, thin aluminum backing for added strength in the field and for a standard UL rate-able product line were demonstrated. Also, critical product certification equipment was procured and validated, and products were demonstrated in selected market sectors to obtain early customer feedback.

In Phase III, renewed emphasis was placed on identifying and correcting the parameters limiting the yield and ultimate efficiency of production cells fabricated on stainless steel. Numerous tests were conducted on the CIGS deposition parameters with the aid of Design of Experiment (DOE) methodology. As a result of these tests, more robust areas of the parameter space were identified and the process was re-baselined. The re-baselining allowed GSE to demonstrate small area test cells with efficiency exceeding 12% and production cells with efficiency greater than 10%.

A program to evaluate the feasibility of Ga effusion rate control by Atomic Absorption Spectroscopy (AAS) was also conducted. Once specific engineering issues related to thermal expansion, optical coating, and baseline drift were properly addressed, the AAS Atomicas system successfully provided good and reproducible Ga flux measurements for CIGS production. Furthermore, the use of standard control algorithms to provide setpoints in a closed-loop multiple level controller was sufficient to demonstrate the utility of AAS in providing Ga thickness control during CIGS deposition. The primary challenge to implementing the sensor in a production environment is the elimination of window coating that occurs during long depositions.

1.0 CIGS ABSORBER IMPROVEMENT

GSE has developed a manufacturable roll-to-roll process for absorber deposition on a 15 cm wide substrate by co-evaporation using a highly efficient source design. The overall objectives have been to optimize the electronic quality of the absorber material and to improve and scale up the source design for four source co-evaporation over a large area (33 cm × 300 meter rolls of substrate) with adequate uniformity. Key issues with absorber improvement are: control; reproducibility; materials utilization for the metals of greater than 50%, and a deposition rate that allows 10 cm/minute roll coating speed.

1.1 Deposition Process Optimization

The deposition parameters for the CIGS layer by four-source co-evaporation were optimized to obtain sequentially higher electronic material quality over larger areas. Adequate adhesion and deposition rates (10 linear cm/min) were maintained. Initial optimization was done on 15 cm substrate widths, progressing to full 33 cm × 300 meter substrate rolls. Deposition parameters that were varied for optimization included substrate temperature profile, selenization delivery profile, and final elemental composition.

CIGS process development was performed exclusively on the production systems during Phase III of the program. Over 50 deposition tests were conducted between the CIGS 1 and CIGS 2 deposition systems using established Design of Experiment (DOE) techniques. The majority of the tests utilized 2- and 3-level factorial designs. The factors tested for included substrate heater temperature, CIGS thickness, NaF thickness, delivery profiles, Se flux, and web speed. Many of the tests were repeated due to inadequate control resulting from unexpected interactions and equipment failure.

In a typical test with a 3-level factorial design with at least nine treatment conditions (replicate test conditions were almost universally appended to the tests), each test condition was maintained for 20-40 feet of web to ensure that the system was stabilized at the new treatment conditions. An in-situ web marker was applied to delineate between test conditions. The typical web coated during a designed experiment was 300 feet in length. After each CIGS deposition process was complete, the web was removed from the chamber and mounted on a motor-driven inspection table. Samples for EDS and SEM analysis were extracted at each treatment condition across the width of the web by referencing the markings on the web. Three 4-in. × 4-in. coupons were also extracted at each location across the web width for device fabrication. Fifty 0.68cm^2 devices were fabricated on each pad and the diode parameters were averaged for analysis. Occasionally, filtering was applied to remove devices well outside the main distribution (shunted) before averaging. Generally, only the center diode pads were analyzed; most control points are referenced to this location. Generation of tests and analyses of test results were conducted with the aid of the DOE module in the Statistica software package.

A report was generated with each DOE completed. A sample of data from a typical report is shown for Test G20178 – a test of substrate heater temperature performed in CIGS 2. Table 1.1

lists the treatment conditions. Figures 1.1 and 1.2 show the cross-sections of CIGS films generated, indicating larger grain size at the higher substrate heater temperatures. The illuminated JV data for each diode pad is shown in Table 1.2. An ANOVA table for a minimized model fitting linear, quadratic, and cross terms is shown in Table 1.3, indicating good fit for efficiency. In this instance, H2T had the strongest effect on efficiency (higher substrate heater temperature, higher efficiency).

Interactions between JV parameters were also analyzed. Larger V_{oc} and fill factor were obtained at the high H2T condition, but were partially offset by a reduced J_{sc}, probably due to enhanced Ga diffusion towards the junction under that condition (Figures 1.3 and 1.4).

At the conclusion of this intensive round of designed experiments, an optimized set of deposition conditions was down-selected for incorporation as baseline process conditions.

Table 1.1: Test treatment conditions (G20178 – CIGS2 – 577SA)

TTMT	H1T	H2T	H3T
10	M	M	L
9	H	M	M
8	H	L	H
7	H	H	L
6	M	M	H
5	M	L	L
4	M	H	M
3	L	M	L
2	L	L	M
1	L	H	H
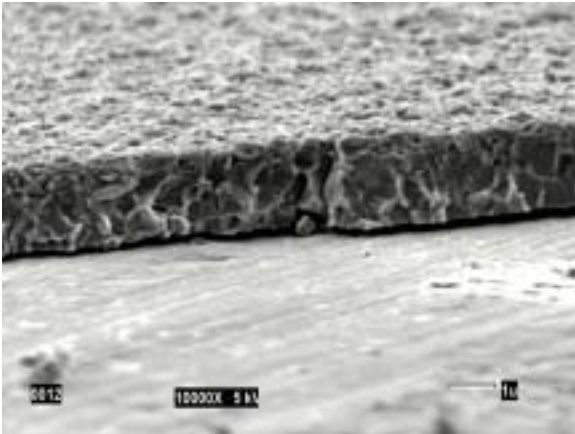
Figure 1.1: X-section SEM of CIGS, treatment 4
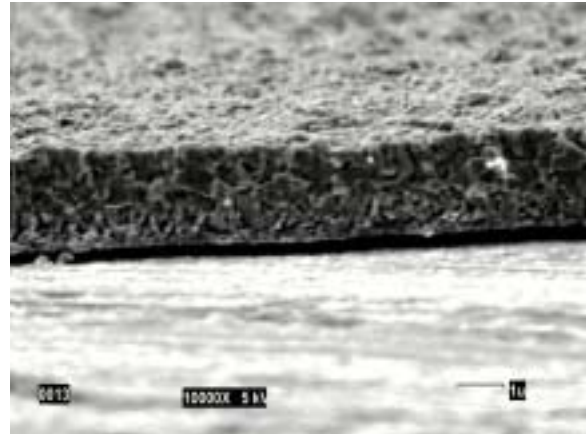
Figure 1.2: X-section SEM of CIGS, treatment 5

Table 1.2: Center diode JV data summary (577SA)

TTMT	V_{OC}	J_{SC}	FF	η
10	589.	18.4	57.8	6.3
9	602.	19.2	62.7	7.3
8	563.	26.3	64.5	9.5
7	598.	16.8	66.6	6.7
6	597.	19.6	65.9	7.7
5	529.	25.9	47.4	6.5
4	572.	26.6	56.9	8.7
3	548.	26.6	47.6	7.0
2	525.	21.2	48.0	5.4
1	514.	28.6	60.9	9.0

Table 1.3: ANOVA; Var.:EFF; R-sqr=.99244; Adj.:.97731
3 3-level factors, 1 Blocks, 10 Runs; MS Residual=.0393164

		SS	df	MS	F	p
(1)H1T	L	.81039	1	.810387	20.61195	.020008
(2)H2T	L+Q	3.03025	2	1.515125	38.53675	.007252
(3)H3T	L	1.29793	1	1.297929	33.01243	.010472
1*2		2.26313	1	2.263129	57.56200	.004751
1*3		1.22893	1	1.228928	31.25740	.011302
Error		.11795	3	.039316		
Total SS		15.59741	9			
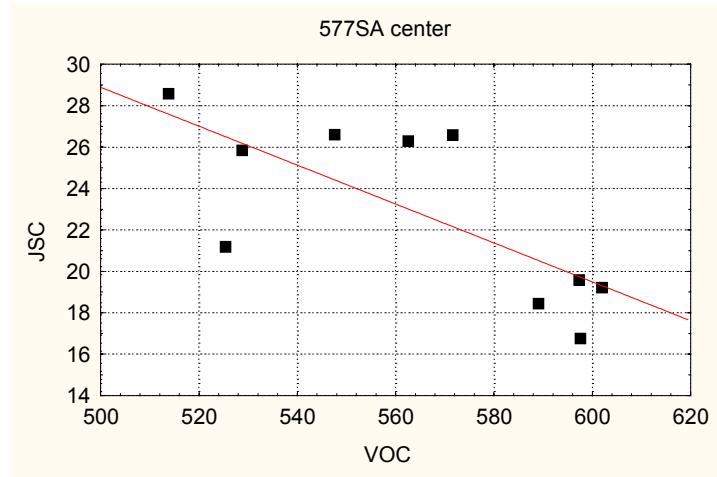
Figure 1.3: JSC as a function of VOC for center diodes

8
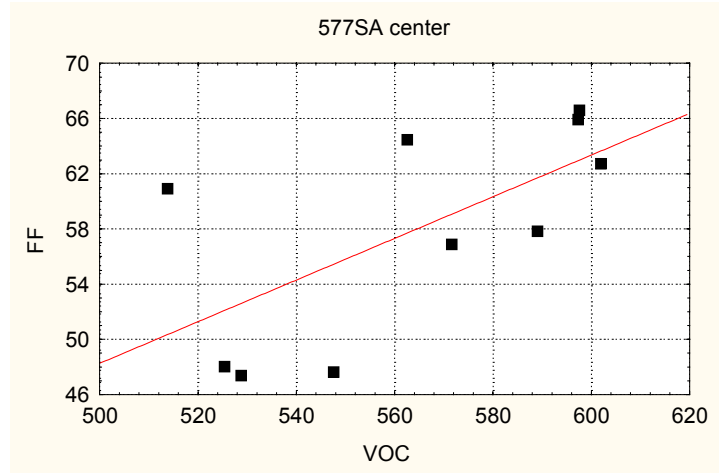
Figure 1.4: FF as a function of VOC for center diodes

1.2 Source Scale-up

GSE's task was to design, fabricate, test and implement scaled-up effusion sources for deposition on 33 cm substrate width (for roll coating 33 cm × 300 meters of substrate) based on existing proven designs used on 15 cm substrate widths. Effusion profile and rate modeling were done in collaboration with the Institute of Energy Conversion, University of Delaware, as a subcontractor. GSE also produced sources for co-evaporation that are mechanically and electrically robust and allow tight flux rate control and spatial uniformity over the substrate width. The GSE sources are very efficient to eliminate heat load on the substrate and system parts (dissipating less than 2.6, 1.5 and 1.2 kW for the Cu, Ga and In sources, respectively, in the 33 cm size).

A special meeting was convened in Denver at the ITN facility on April 18, 2000, to discuss key issues of the GSE effusion sources and identify a path to incorporate desired improvements. Participants from IEC (R. Birkmire, W. Shafarman), Colorado School of Mines (R. Kees, L. Raja, J.P. DelPlanque, M. Pavol), ITN (P. Meyers, B. Lanning, N. Gomez, M. Misra, B. Joshi) and GSE (J. Britt, R. Wendt, D. Graddy) were present.

GSE gave a status report on production effusion source performance. CSM presented the early results of numerical modeling of the GSE effusion sources and detailed areas potentially needing improvement. IEC presented experimental data generated from effusion sources based on GSE designs. IEC agreed to perform additional tests to identify potential areas for effusion source improvements.

The GSE CIGS deposition process relies on discrete effusion sources to deposit Cu, Ga, and In on a web. Cross-web CIGS compositional non-uniformity can be attributed to thickness non-uniformities from one or more individual metal sources; identification of malfunctioning effusion sources is the first step toward eliminating cross-web non-uniformities.

Measuring the thickness of CIGS films or CIGS precursor films was problematic, however. The thickness of coatings on stainless steel web is difficult to accurately measure by profilometry;

9

scratching the thin films to form a step deformed the relatively soft stainless steel and induced measurement error. While cross-section SEM is routinely used to determine CIGS thickness, the Selenide precursor films were too thin to accurately measure with the GSE SEM.

GSE investigated the use of EDS to qualitatively estimate the variation in precursor film thickness across the web. The technique consists of applying EDS at an accelerating voltage of 20 kV and expressing the concentration of Mo (back contact) as atomic percent. Assuming the Mo thickness is constant, an increase in Mo atomic percent from one location to another corresponds to a decrease in coating thickness. The variation in Mo atomic % across the web width for "thick" and "thin" $(In,Ga)_2Se_3$ films (Figure 1.5) shows a trend of decreasing coating thickness towards one edge of the web in both cases. This behavior was observed repeatedly and believed to be endemic to the GSE effusion source design.
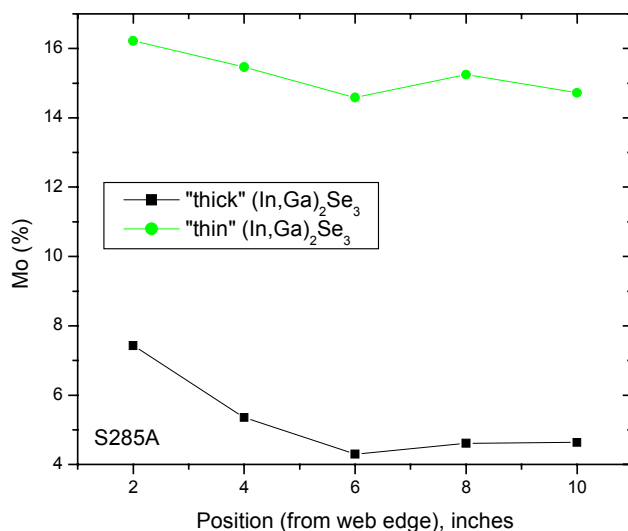
Figure 1.5: Variation in Mo atomic % across the web width for "thick" and "thin" $(In,Ga)_2Se_3$

A later generation production effusion source design was evaluated for cross-web uniformity over a range of temperatures. The evaluations were performed in a GSE research chamber by evaporating Cu onto glass slides attached to a web translated at production speeds above the effusion source; Cu thickness on the glass slides was then evaluated by profilometry. The non-uniformity at a particular effusion source temperature, defined as the standard deviation divided by the mean, ranged from 2.3% to 5.8%. The min-max difference divided by the mean at a particular temperature ranged from 8.2% to 16.7%. The results (Figure 1.6) indicate that cross-web non-uniformity is temperature dependent. Best uniformity was achieved for Cu thicknesses between 1000-2000Å.

An updated status report with emphasis on then outstanding problems was presented at the Effusion Source, Sensor and Control Meeting held at IEC, University of Delaware, on July 7, 2000. Participants included the Institute for Energy Conversion, Colorado School of Mines,

ITNES, and GSE. Effusion source status was declared adequate but in need of advanced designs for higher rates and longer runs; sensor/controls issues were deemed to need more immediate attention.
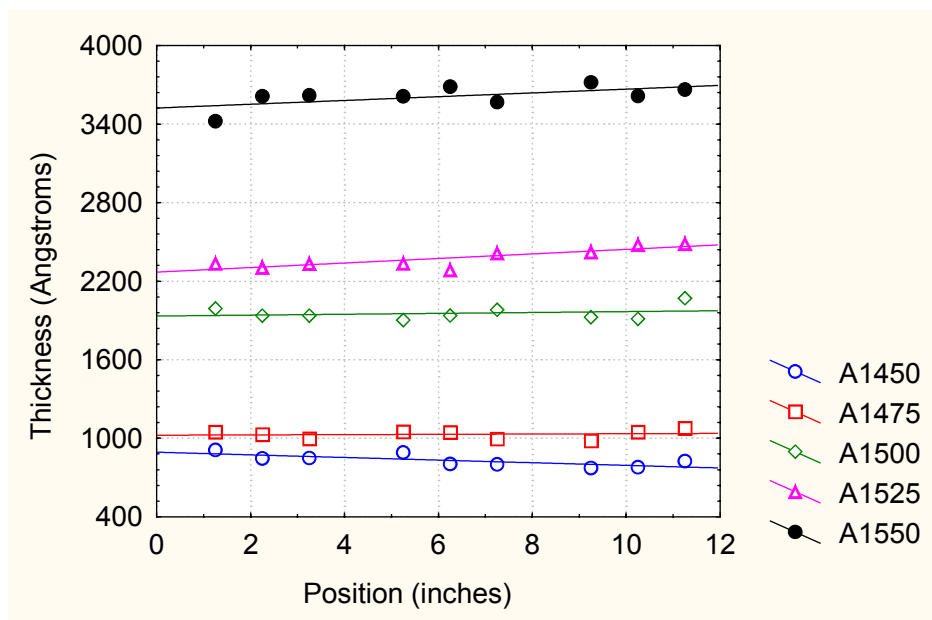
Figure 1.6: Cross-web Cu thickness as a function of effusion source temperature

Intensive analyses of production CIGS composition and thickness continued; Figure 1.7 shows a histogram of Cu/(Ga+In) for approximately 45 production lots. It was found that cross-web composition control related to effusion sources was a larger source of variation than along-web.
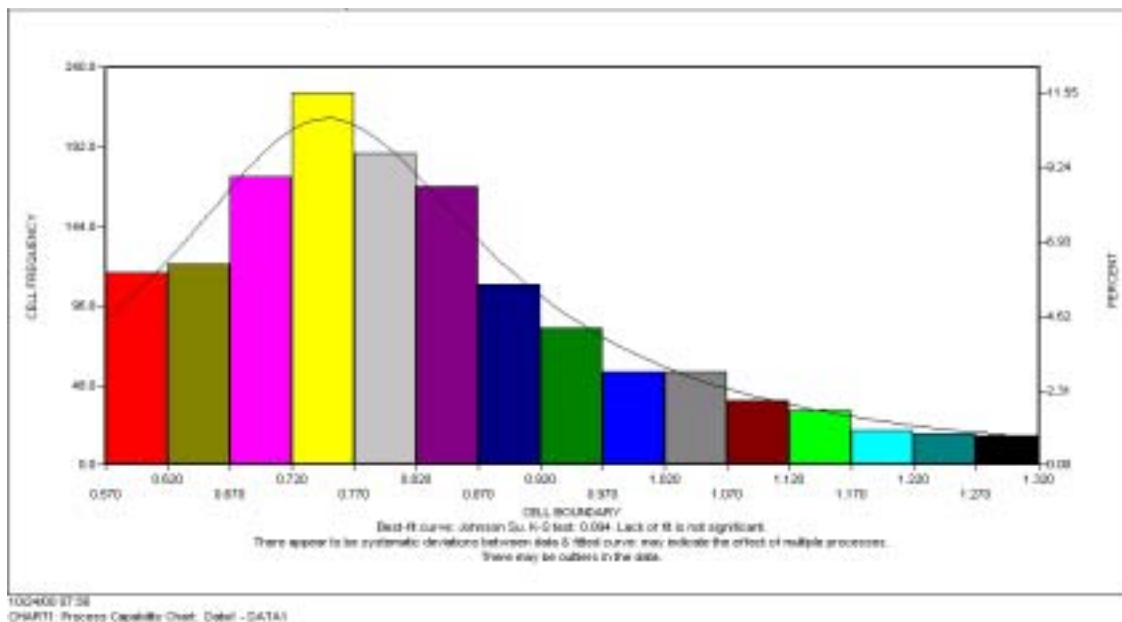
Figure 1.7: Cu/(Ga+In) histogram, production CIGS

Continued improvements in cross-web compositional uniformity were achieved in the production coaters through operational procedures and minor design modifications to the standard effusion source. Many runs demonstrated cross-web compositional uniformity within established specification limits (Figure 1.8); the uniformity was sufficient to meet the manufacturing and program goals.
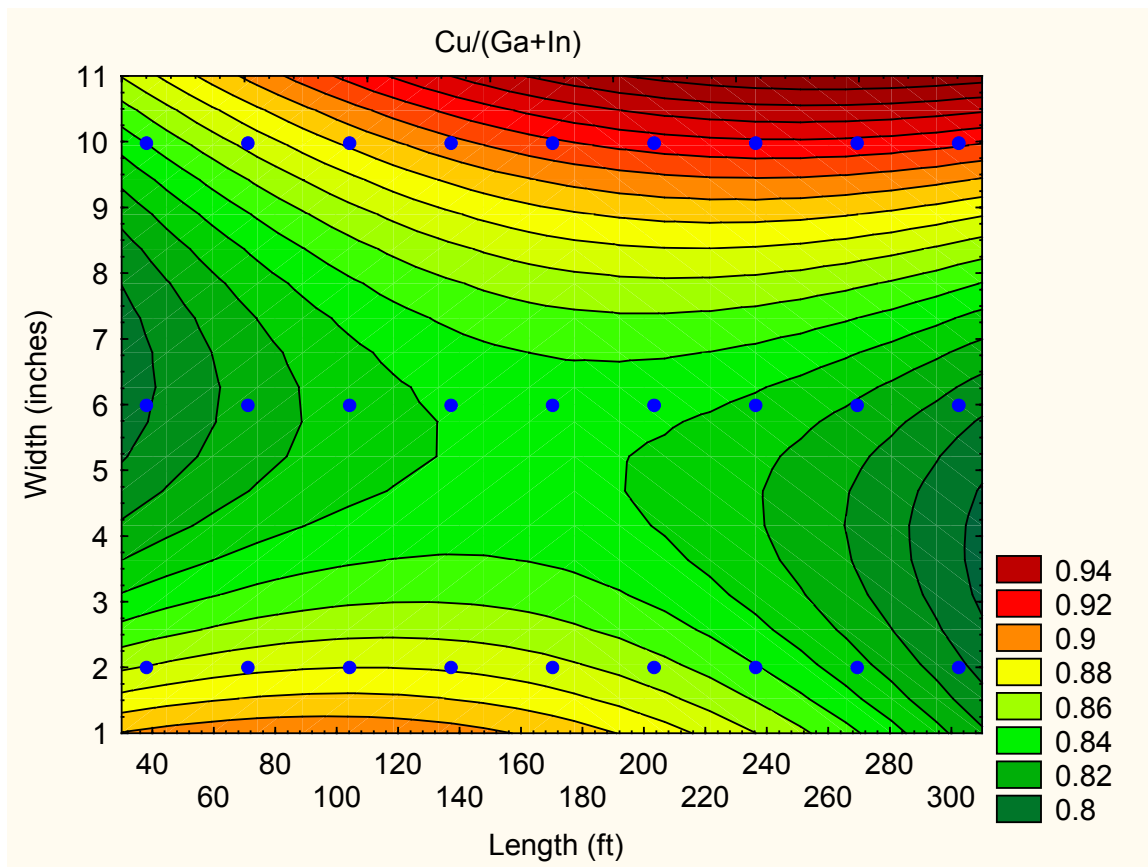
Figure 1.8: Cu/(Ga+In) contour map for lot 517SA

1.3 Efficiency Improvement Studies

Absorber quality optimization progressed sequentially to attain higher efficiencies and larger areas, beginning at a small area device efficiency goal of 10% on 15 cm substrate widths, and continuing with larger (33 cm wide) substrates and scaled-up sources, to 12.0% and 13.0% device efficiency. Beyond that point, efficiency optimization shifted to the cell level.

An investigation concerning potential impurities in the CIGS arising from the stainless steel substrate was launched. The extrinsic addition of sodium during film growth was also further investigated as a means to enhance grain growth, carrier concentration and electronic quality of the absorber layer. This addition of Na was effected by direct co-evaporation of a sodium

compound. Both investigations were performed with the assistance of the Institute of Energy Conversion at the University of Delaware under subcontract.

Diffusion of stainless steel components into the CIGS is a source of concern. In a series of tests conducted at IEC, types A and B stainless steel were compared as substrates for CIGS deposition, with stainless steel coupons provided by GSE. Types A and B stainless steel had substantially different base constituents. An identical Mo film, approximately 1 μm thick, was applied to each substrate. CIGS films were deposited at substrate temperatures of 400°C and 550°C without extrinsic Na doping. The CIGS films on the (2-in. × 2-in.) substrates were also fabricated into devices and characterized at IEC. The JV results are shown in Table 1.4. At the higher substrate temperature, the devices fabricated on type B stainless steel proved superior to those on the type A steel. At the lower substrate temperature, the substrates were roughly equivalent, but with low efficiency. CIGS samples from each set were measured by SIMS at the University of Illinois (A. Rockett) to estimate the diffusion of stainless steel components into the CIGS (see Figures 1.9 – 1.12).

As a result of the IEC tests, the following conclusions were drawn:
The SIMS measurements showed a significant amount of stainless steel components in the CIGS films but not in the Mo.
Less Fe and Cr are found in CIGS deposited on type B stainless steel than on type A SS at both the high and low substrate temperatures.
Fe, Cr, and Cu are all found in much higher concentrations in the Mo deposited on type A SS at the high and low substrate temperatures.
The overall highest device efficiency on SS was on type B with CIGS deposited at 550°C.
At a substrate temperature of 400°C, device efficiencies were better on the type A SS.

Table 1.4: Stainless steel alloy JV results

550°C, No Na Doping				
Substrate	V_{oc} (mV)	J_{sc} (mA/cm^2)	FF (%)	Efficiency (%)
Type A SS/Mo	0.288	7.9	30.3	0.7
Type B SS/Mo	0.485	32.2	54.4	8.5
SL glass/Mo	0.575	32.9	70.7	13.4
400°C, No Na Doping				
Substrate	V_{oc} (mV)	J_{sc} (mA/cm^2)	FF (%)	Efficiency (%)
Type A SS/Mo	0.509	24.2	51.7	6.4
Type B SS/Mo	0.384	25.1	39.4	3.8
SL glass/Mo	0.585	30.3	62.8	11.1
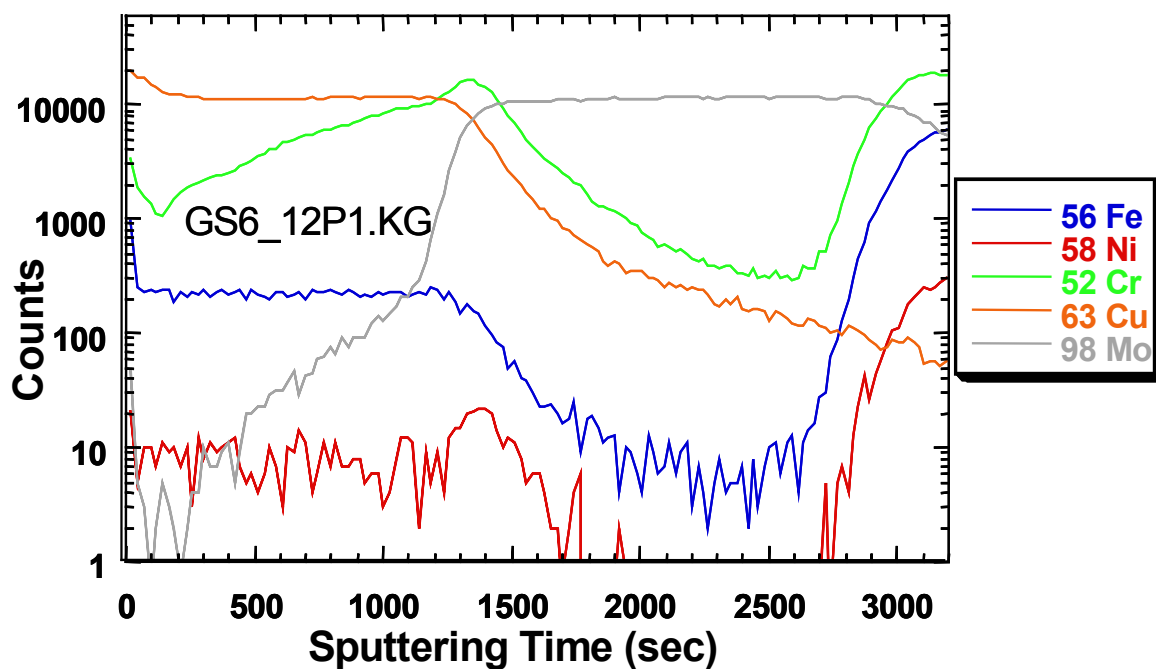
Figure 1.9: Using type A stainless steel as the substrate for CIGS deposition, at a substrate temperature of 550°C, the Cu signal in the Mo indicates significant intermixing. Very high Cr is present in the CIGS, as well as Fe and significant Ni.
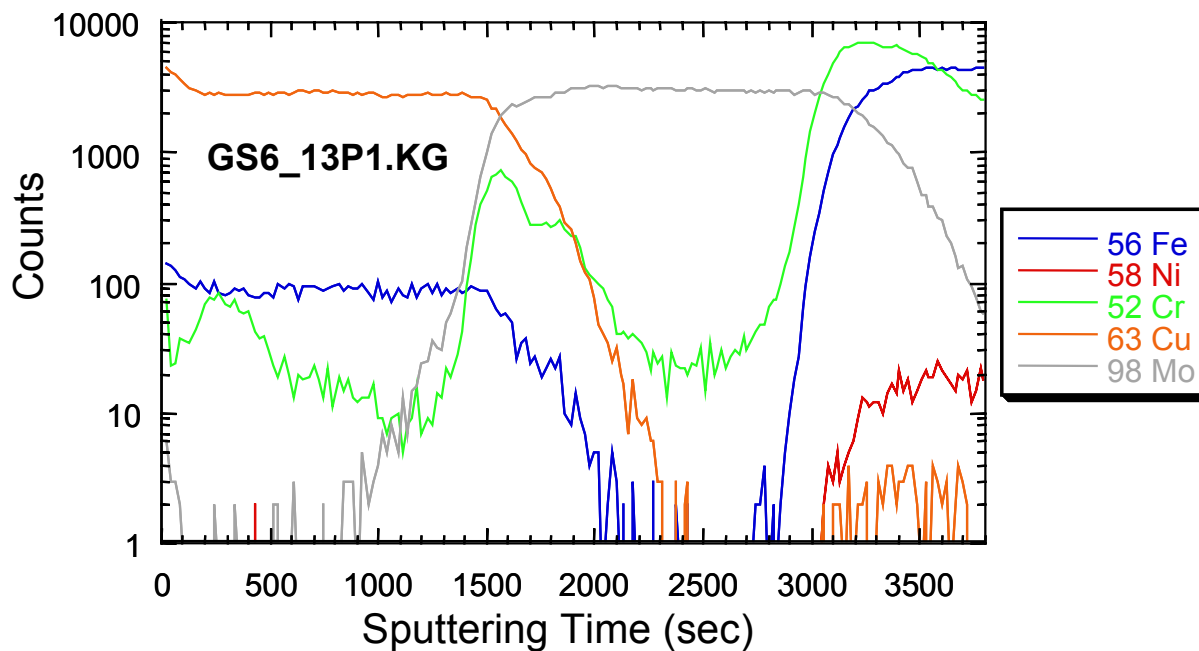
Figure 1.10: Using type B stainless steel as the substrate for CIGS deposition, at a substrate temperature of 550°C, a fairly abrupt Cu decrease indicates little Cu is moving into the Mo. There is also less Cr in the Mo and in the CIGS. Fe is present in the CIGS but Ni is insignificant.
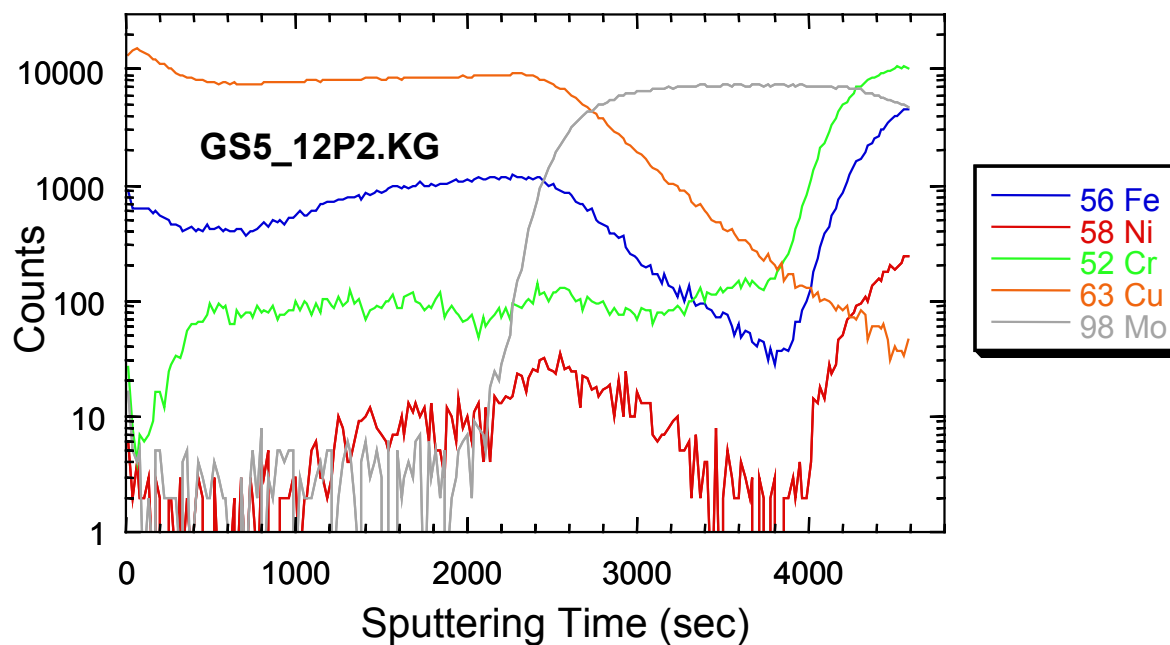
Figure 1.11: Using type A stainless steel as the substrate for CIGS deposition, at a substrate temperature of 400°C, the Cu signal in the Mo indicates significant intermixing. There are more Fe and Cr in the CIGS than with type B SS, but there is much less Cr than at a substrate temperature of 550°C.
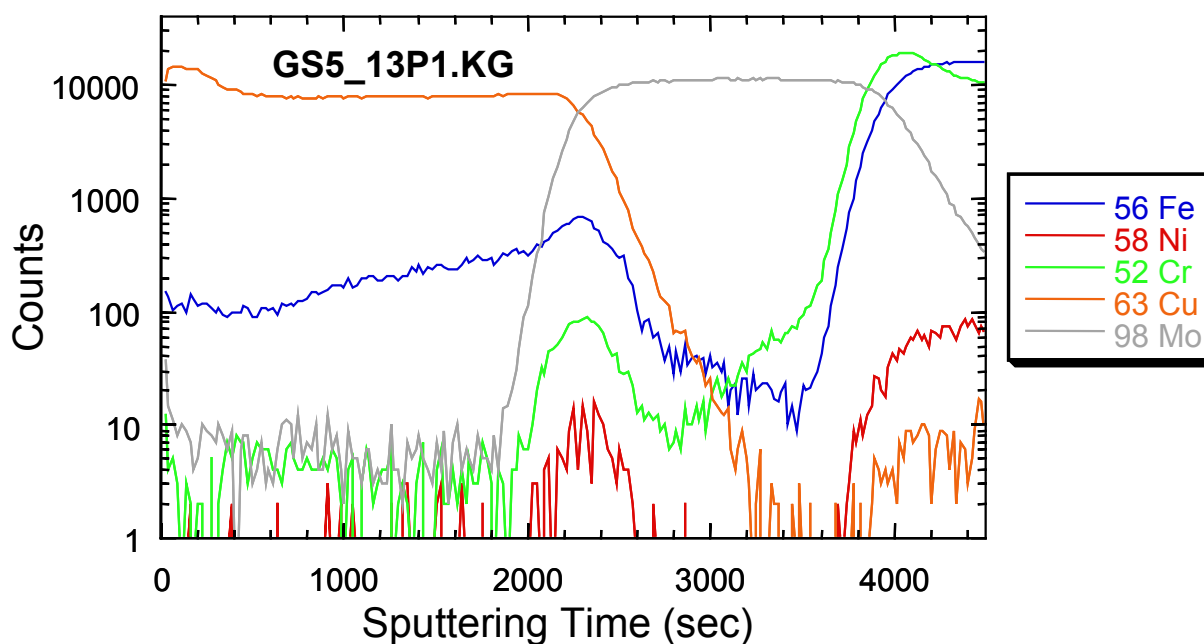
Figure 1.12: Using type B stainless steel as the substrate for CIGS deposition, at a substrate temperature of 400°C, less Cu is intermixed in the Mo, and there is insignificant Ni in the CIGS. Only Fe is present in a significant amount.

1.3.1 Na Incorporation

In response to severe yield losses in the Final Assembly area, caused by delamination of CIGS films from the Mo substrate, a special investigation was initiated. The interface at which adhesion failure occurred was determined from EDS analyses. The adhesion failure was found to occur between the Mo and CIGS. A reliable scratch technique for characterizing the adhesion of CIGS films was developed (Figures 1.13a and 1.13b), historical lots were evaluated, suspected causes of adhesion failure were proposed, and special test runs were completed and analyzed. Statistical analysis then was performed to identify possible correlation between suspected process variables and material characteristics.

ICP was employed to determine the integral composition of samples that exhibited good, medium, and poor adhesion, according to the scribe method used at GSE to evaluate adhesion. Investigation of a possible correlation between CIGS adhesion and Na content (determined by ICP) was also done. A multiple regression analysis to determine the correlation of suspect variables to adhesion scratch width was performed on the data set.

A result of this investigation was the significant positive correlation found between Na concentration and poor adhesion. Figure 1.14 shows the relationship between adhesion and Na concentration. All films with poor adhesion were found to have greater than 0.4 atomic % Na.
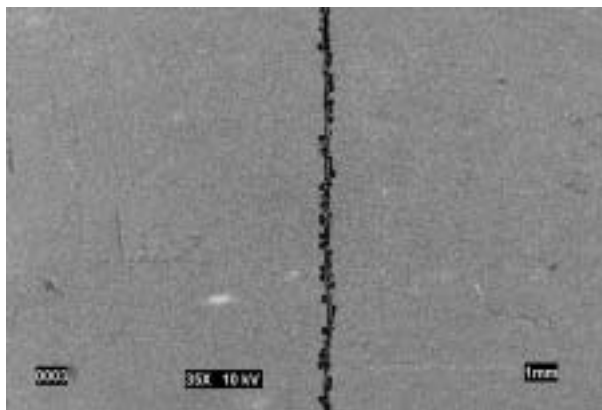
Figure 1.13a: Scratch test exhibiting good adhesion

Figure 1.13b: Scratch test exhibiting poor adhesion
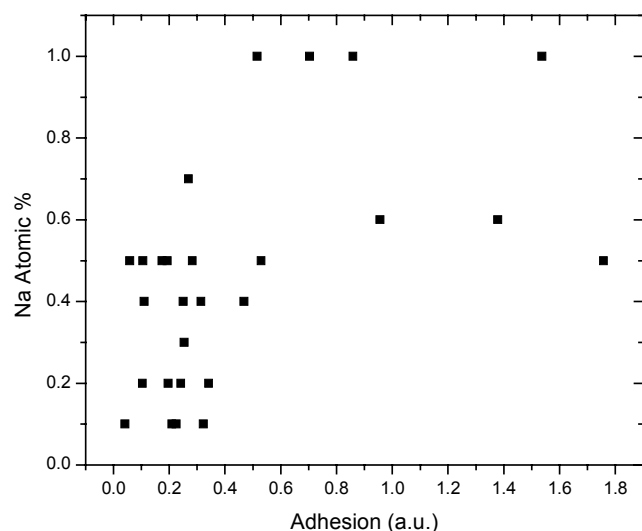
Figure 1.14: CIGS adhesion as a function of Na concentration

The sensitivity of adhesion and efficiency to Na concentration prompted an investigation of the cross-web thickness uniformity of NaF in our CIGS production chambers.   The cross-web thickness uniformity of the NaF coating was determined by effusing NaF at 1.8Å/s onto a stationary web to which witness glass slides had been attached in three rows covering the edges and center of the 6-in. long and 13-in. wide deposition window. Dektak thickness measurements were taken at the distances from the reference edge as listed in Table 1.5. The data indicates a cross-web thickness deviation of 15 to 23% at the edges relative to the center position.

Table 1.5: NaF cross-web thickness uniformity as determined by Dektak measurements

Row #	45	70	145	170	245	270	average	1σ
	Distance from the reference edge in mm		
	NaF thickness in Å		
1	7807	7458	7828	7281	6779	6949	7350	434
2	10502	9918	12850	13109	10286	9629	11049	1527
3	9543	9754	11897	11169	8246	8538	9858	1437
average	9284	9043	10858	10520	8437	8372	9419	1133
1σ	1366	1375	2667	2968	1761	1348	1888	607

Prior to optimizing the NaF precursor thickness, tests were conducted to determine the stability of the deposition rate during CIGS deposition. Figure 1.15 shows the sensor signal for 280 ft. of CIGS deposition during which the control rate was set to 2.0Å/s – this rate corresponds to a NaF thickness of 120Å.

17

Na incorporation into the CIGS film was verified via ICP analysis of CIGS deposited onto NaF precursors of different thicknesses. The plot in Figure 1.16 shows that the Na level detected in the samples increased with an increase in NaF thickness (i.e., NaF rate). The relationship was found not to be linear; rather, the initially exponential increase approached a saturation limit. Na concentration was consistently greatest in the center of the web – most likely due to a non-uniform flux profile caused by non-optimal effusion source design.

No statistical difference in device efficiency was obtained for Na incorporation at various levels and under several CIGS deposition conditions. However, CIGS deposited on NaF precursors of different thicknesses did result in a decrease of the CIGS to back contact/substrate adhesion at the 10 to 14% level.
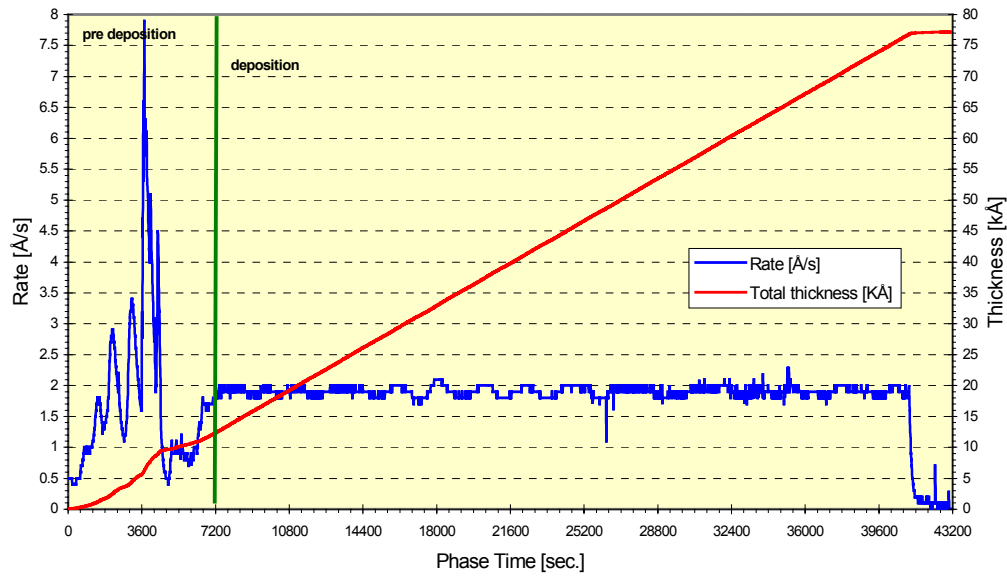
Figure 1.15: NaF rate controlled at 2.0Å/s for 280 ft. of CIGS deposition
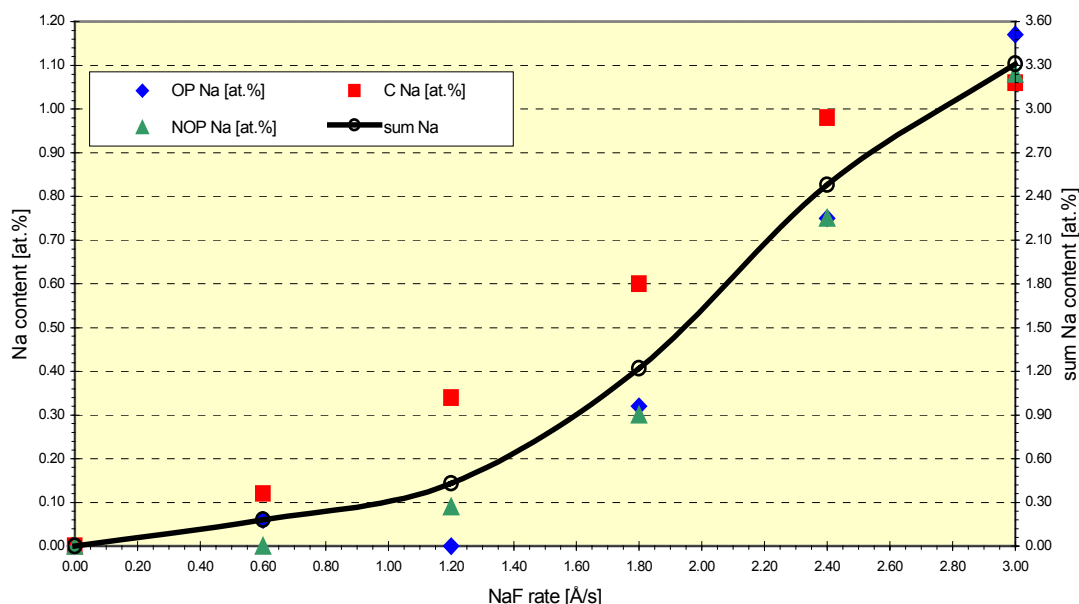
Figure 1.16: Na incorporation into CIGS as a function of NaF rate

As sodium has been found to improve device efficiency at concentrations near 1% in CIGS devices, further investigations at GSE focused on the use of substrate type B. This approach eliminates the detrimental impurity outdiffusion previously limiting the benefits of intentional Na incorporation into the absorber. Subsequently, the most efficient devices made at GSE on stainless steel substrates have been made with extrinsic Na added (Figure 1.17). As was the case on the type A steel, an excess of sodium degrades CIGS adhesion to the substrate. Thus, the intentional incorporation of Na must be carefully controlled.

A comparison of the amount of Na detected by SIMS analysis on 'Na-free' CIGS on type B SS vs. absorbers with intentional Na incorporation is illustrated in Figure 1.18. Also plotted is the Na level detected in a CIGS absorber deposited onto SLG substrate at NREL. The remaining Na signal above the background level for the web sections that were not intentionally exposed to the NaF flux is an artifact of the experimental approach. These data points correspond to the half of the substrate that was shuttered from direct NaF flux. However, the data indicates that small amounts of NaF reached the substrate despite the shutter.

Corresponding device efficiencies for CIGS having different levels of Na, along with the signal monitored for the Na flux and the actual incorporated Na level in the CIGS prepared on SS substrates, is shown in Figure 1.17. The data there shows the average efficiency of many devices, and indicates a monotonic increase in efficiency over the range studied. Investigation of extrinsic Na introduction will continue to obtain more definitive data over a greater range and to further optimize efficiency.
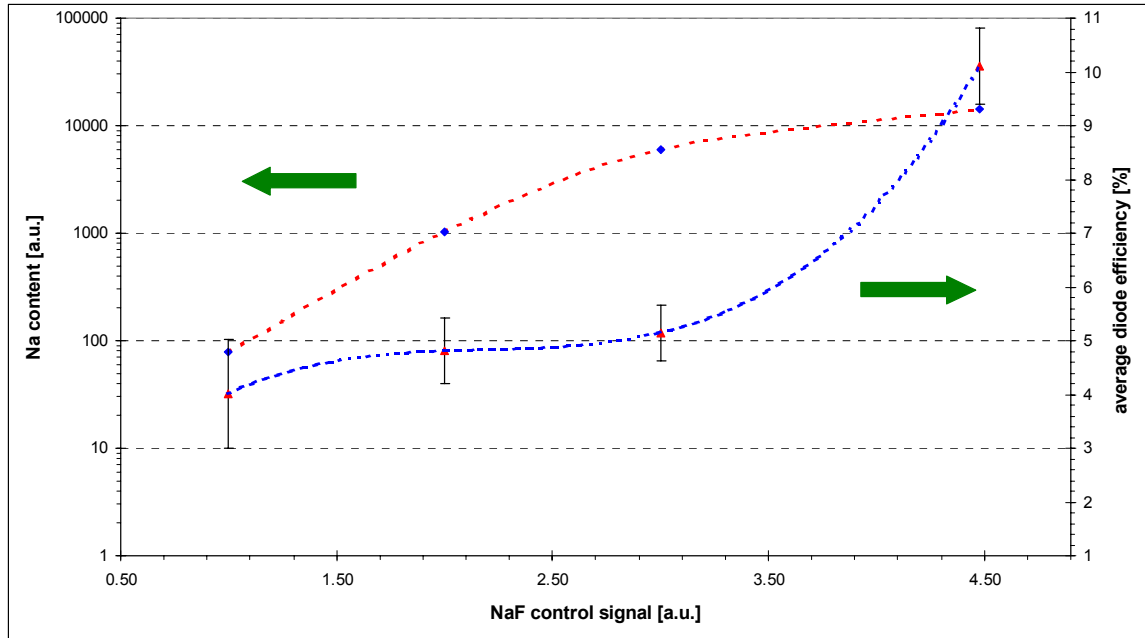
Figure 1.17: Sodium content measured in the absorber by SIMS is related to average device efficiency and the sensor signal monitoring Na flux during deposition
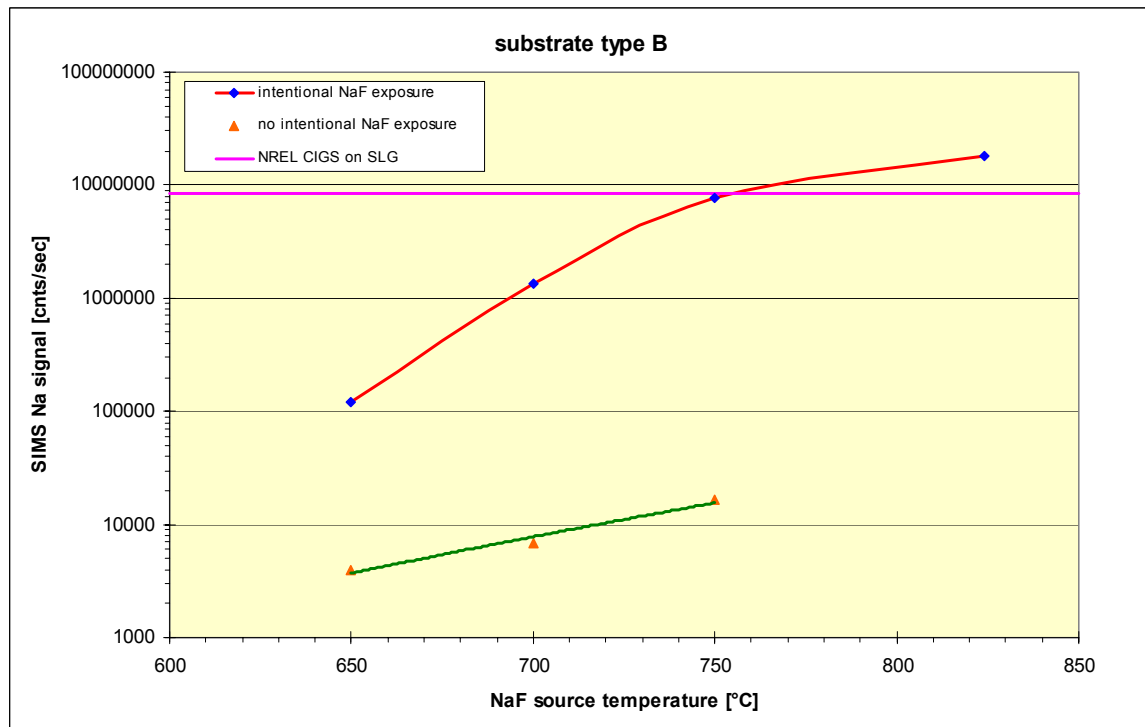
Figure 1.18: Sodium content measured in the absorber by SIMS for intentional Na incorporation, the shuttered 'Na-free' half, and CIGS on SLG deposited at NREL

20

1.4 Heterojunction Formation Capability

Small area device results were monitored throughout the program to ensure process compatibility between absorber deposition and heterojunction formation. The vast majority of lots coated with CIGS were completed through all thin film deposition steps. Five hundred to 1000 small area devices were fabricated on each completed lot at regular intervals along the web, and approximately half of the devices from each lot were characterized by illuminated JV measurements (AM1.5). The results were stored on a process tracking database and reviewed thoroughly for feedback to the process.

Tests of CdS thickness controlled by web speed appeared to indicate that thicker CdS films provide higher efficiencies. Following further verification, the recommendation was made to change the baseline process to a lower web speed to allow a thicker CdS film.

Tests also were conducted to determine the effect of varying ITO thickness on electrical characteristics of fabricated devices and to estimate the optimum deposited ITO thickness in terms of average device efficiency and yield. A web speed greater than the baseline web speed was determined to maximize efficiency; baseline conditions were adjusted as a result. An additional benefit was improvement in the throughput of the ITO process.

To compare CBD CdS buffer layers with the production CdS sputter deposition, a bench top R&D system was designed as shown in Figures 1.19 and 1.20. Up to eight 4-in. × 4-in. specimens were deposited simultaneously; an optical CdS thickness uniformity evaluation using SLG substrates revealed $d_{(CdS)} = 350 \pm 98$Å. The relatively large standard deviation (1σ) was a function of the low sticking coefficient of CBD CdS to bare SLG and potential rinse damage to two of the 16 glass slides. Process details are illustrated in Figures 1.21 and 1.22. First diode results employing CBD CdS on CIGS absorbers of Lot 522SA (301SS) are graphed in Figure1.23. Diode pads from absorber sections adjacent to those coated with CBD CdS were processed through the standard GSE sputter deposition of CdS (Figure 1.24). From these graphs, it is evident that a considerable discrepancy existed between the CBD and sputtered CdS processes.
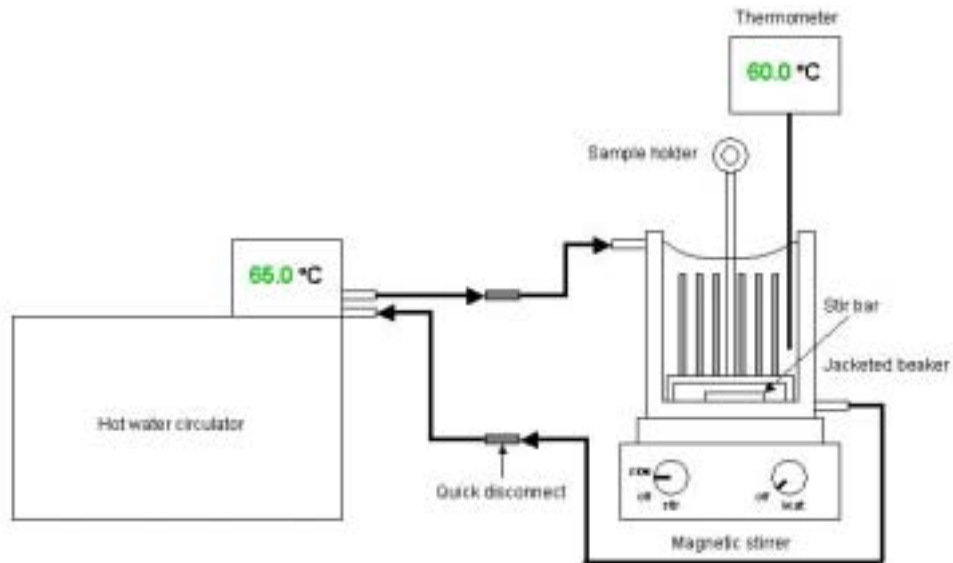
Figure 1.19: Schematic of the bench top R&D CBD CdS deposition setup
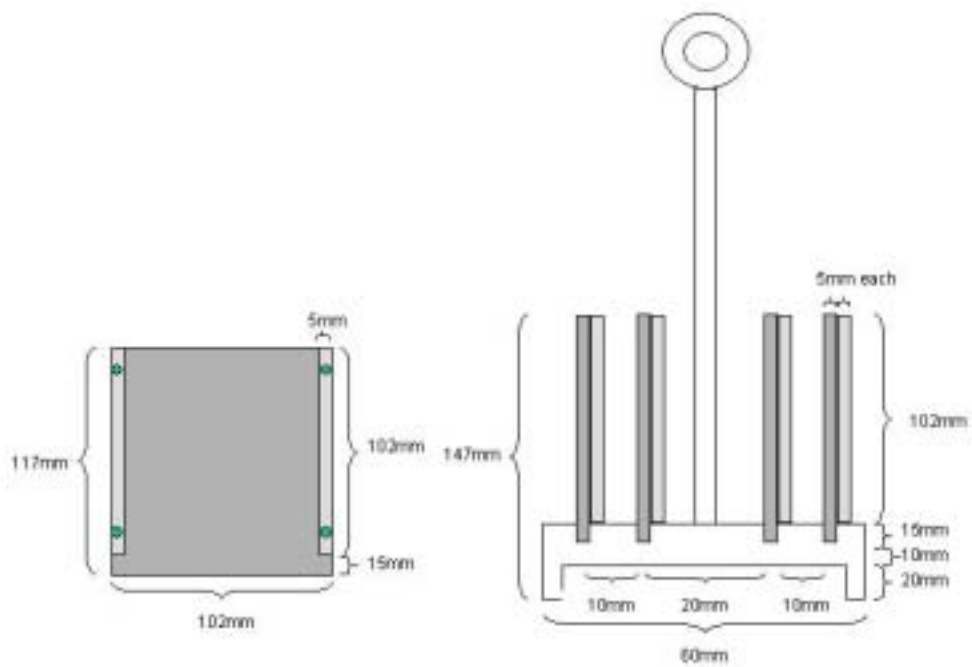
Figure 1.20: Schematic diagram illustrating the sample holder design allowing for deposition of up to eight 4-in. × 4-in. specimens
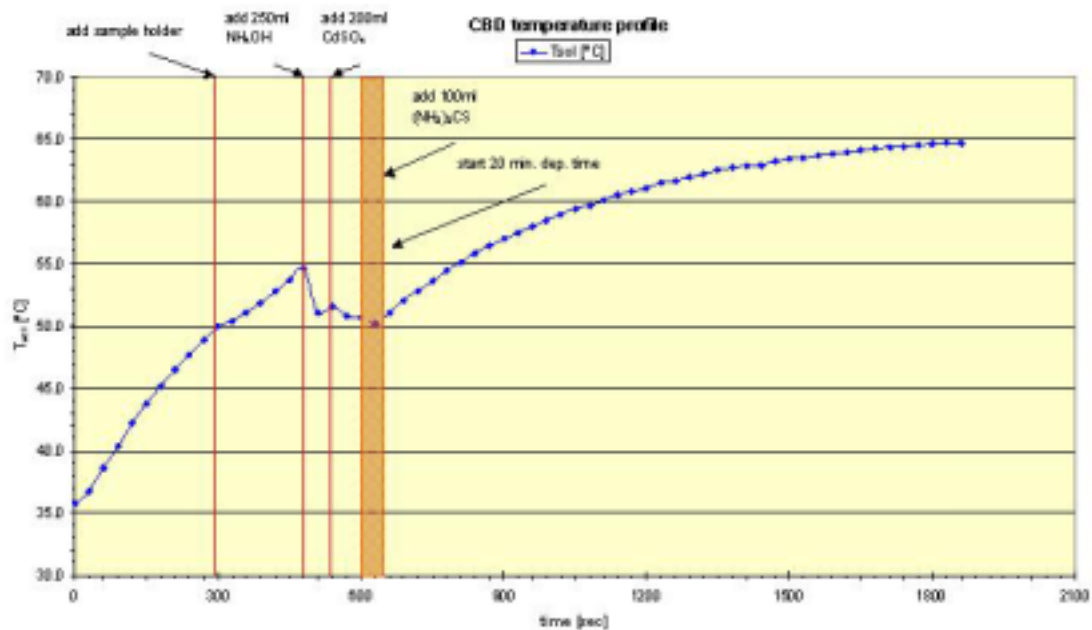
Figure 1.21: Temperature profile of the CBD CdS process as performed at GSE
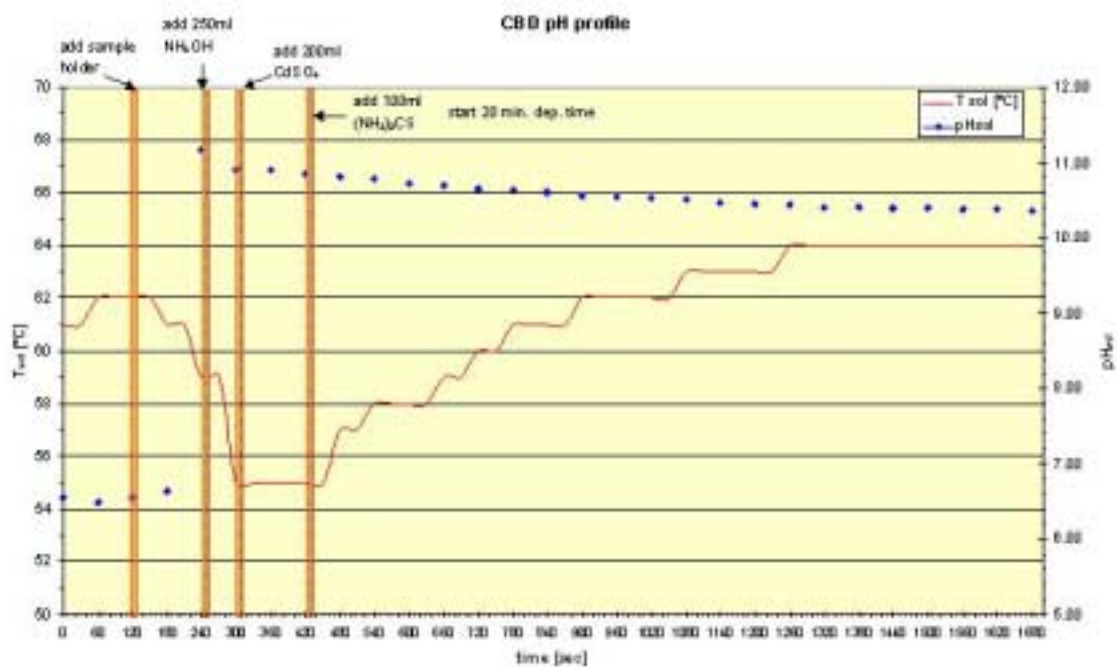
Figure 1.22: Temperature compensated pH and corresponding temperature profile of the CBD CdS process as performed at GSE

23
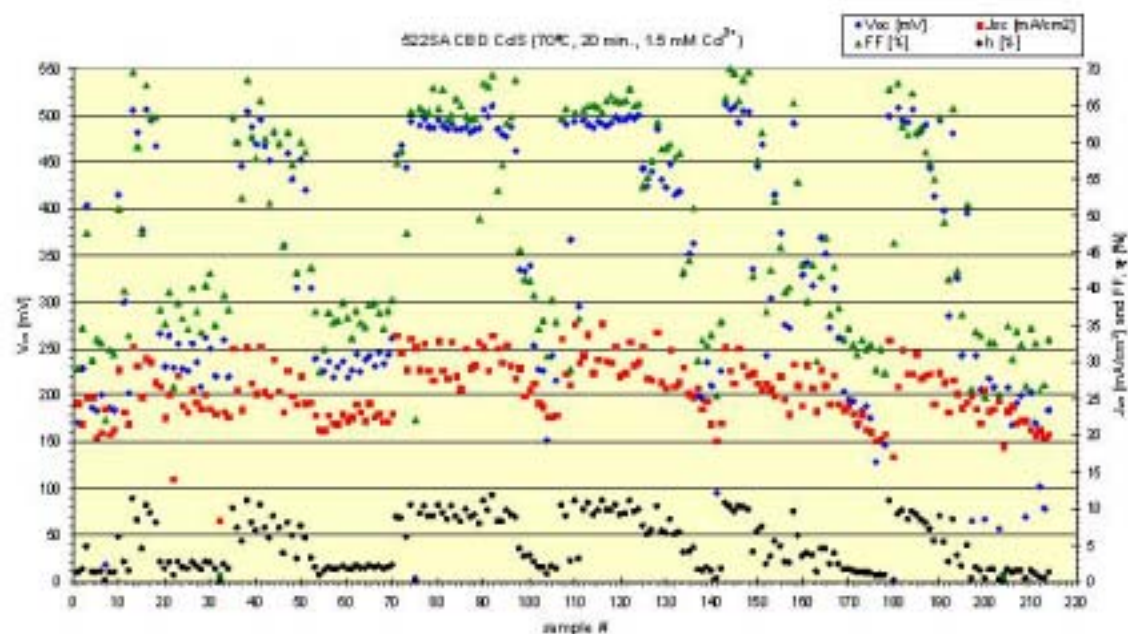
Figure 1.23: Diode parameters for the first set of CIGS-based PV devices processed in the CBD CdS process at GSE

Note: The 70°C process temperature refers to the circulating water bath; actual solution temperature profiles are given in Figures 1.21 and 1.22
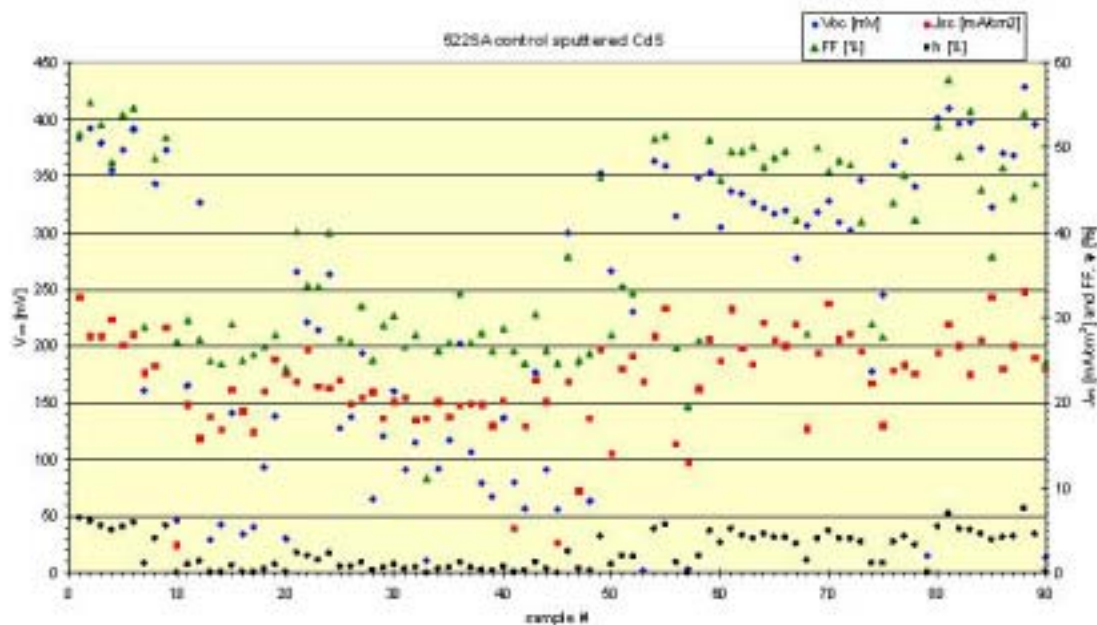
Figure 1.24: Diode parameters employing sputtered CdS; the corresponding CBD CdS data is shown in Figure 1.23

24

Studies comparing the GSE vacuum deposited CdS against the laboratory standard CBD CdS continued through Phase III. The goals were to understand the limitations of the sputtered CdS process and to identify new approaches to match or exceed the performance achieved with the wet process.

A study employing Zn^{2+} and/or Cd^{2+} was conducted. In the first study, the effects of Cd^{2+} PE baths were compared to: (a) standard GSE sputtered CdS; (b) CBD CdS, and (c) thin sputtered CdS. The CIGS absorber used for this study was deposited with intentional Na incorporation. As is evident from Figures 1.25 and 1.26, little to no improvement was obtained when compared to the direct sputter deposition of 600Å CdS onto the absorber. The result with CBD CdS was superior to that achieved with other techniques.

In a subsequent experiment, CIGS films were subjected to various Zn^{2+} PE baths. Direct TCO deposition on PEB treated absorbers did not result in any photoactive devices (Figure 1.27). The addition of 600Å of sputtered CdS did yield photoactive material, but the performance was only about one-half that of CBD CdS finished CIGS, limited mostly by V_{oc} and FF.
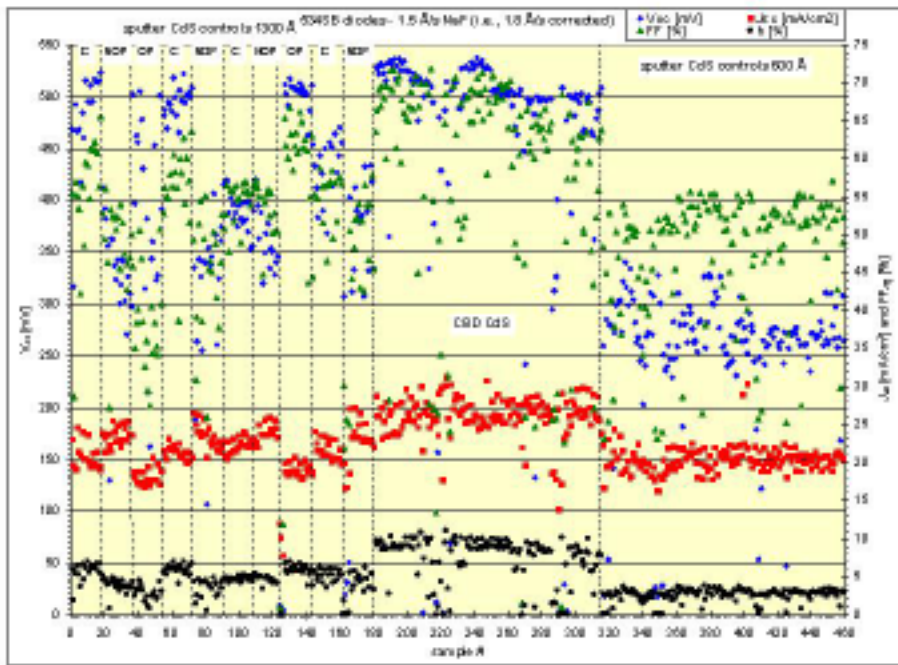
**Figure 1.25: Control diode data on Lot 534SB (intentional Na incorporation) illustrating:
(a) standard GSE sputter CdS 1300 Å; (b) CBD CdS, and (c) non-standard sputter CdS 600Å**
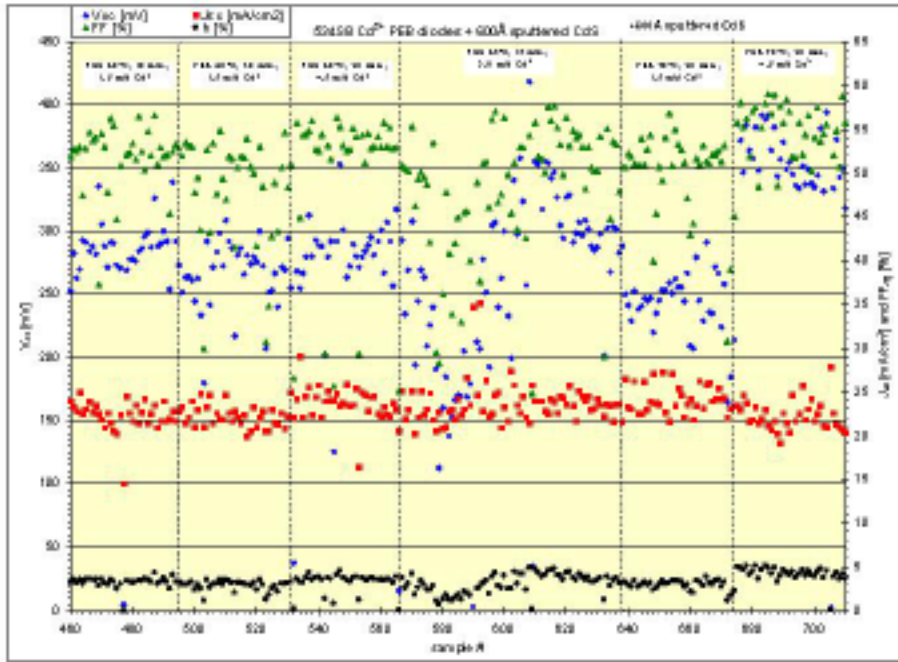
Figure 1.26: Diode data for 534SB after various Cd^{2+} PEB treatments and 600Å of sputtered CdS
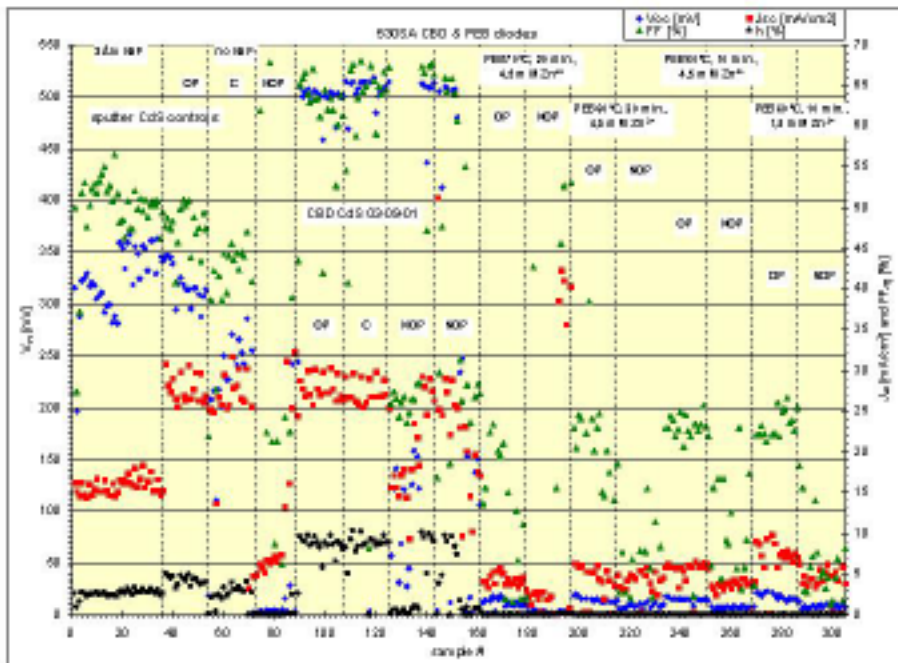
Figure 1.27: Diode parameters for CIGS-based devices employing: (a) 1300Å sputter CdS buffer; (b) CBD CdS buffer, and (c) Zn^{2+} PE (no buffer)

The above demonstrated advantage of the wet chemical CdS buffer deposition over the current RF sputter baseline CdS provides a challenge that is equally important for devices on type B SS. However, GSE's continued commitment to complete roll-to-roll processing of CIGS on flexible substrates is incompatible with the CBD process. Unfortunately, neither a Cd^{2+} nor Zn^{2+} partial electrolyte treatment – with or without a sputtered CdS layer – resulted in device performance improvements rivaling those of the CBD CdS buffer. Future work will be directed toward identifying avenues allowing GSE to combine the beneficial aspects of the CBD buffer process formation with the advantages of roll-to-roll processing.

1.5 Process Scaling and Repeatability

GSE evaluated the reproducibility, stoichiometric uniformity, and thickness of the absorber layer over long (33 cm × 300 meter) runs and from run to run to determine and minimize variability. Uniformity over progressively larger areas was demonstrated using matrices of devices having average efficiency of 12.5% cut from 33 cm × 300 meter rolls of material.

Throughout the program, multiple depositions were conducted to determine CIGS process repeatability. The average length of coated web per deposition was 150 ft. The stoichiometric and thickness uniformity of the CIGS layer from lot to lot was evaluated; process control was determined to be responsible for the majority of the variability observed, with the remainder due to source malfunctioning and operator error.

Several programs were put in place to improve CIGS process control. An atomic absorption spectrometer (AAS) was installed in the production machine to monitor the Cu effusion rate; additional units were procured to monitor In and Ga. Also, substantial modifications were made to the AAS system to successfully integrate it into the hostile deposition environment, where it supplements the thermocouple control of effusion sources.

An X-ray fluorescometer (XRF) was developed as a downstream product sensor. The XRF unit allows in-situ sensing of CIGS composition and thickness and was installed into the pilot CIGS production system. A software control platform that inputs thermocouple, Atomic Absorption Spectroscopy (AAS), and other sensor data and makes appropriate setpoint changes was installed. Throughout the period, continuous modifications were made to the control strategy as new sensors were installed and additional process insight gained.

The issues of source malfunctioning and operator error were addressed by introducing operator documentation that details exactly how effusion sources are to be assembled and installed, procedures for pre-deposition maintenance, baseline run conditions, and deposition procedures. Repeatability was substantially improved as a result of these actions.

To investigate non-equilibrium changes in thickness and composition during the course of a run, a test run was conducted under constant temperature control and with close monitoring of the AAS signals for Cu and In. It was found that In absorption increased dramatically during the first 60-90 minutes of the run, while Cu absorption decreased. It was also discovered that AAS can provide high accuracy in controlling composition for these two sources.

Extending pre-deposition time as a possible solution to non-equilibrium conditions that exist at start of a CIGS deposition was investigated and led to a 5-10% improvement in yield when implemented. Composition yield was improved through better selection of process baseline conditions and improved control strategies during CIGS deposition.

Numerous tests to meet the goal of >10% average efficiency also were performed. Average efficiencies of only 8% were achieved initially, using baseline manufacturing processes; however, CBD CdS showed great promise for meeting the goal. An assessment of CBD CdS utility was performed using 16 3-in. × 3-in. coupons, which were cut from a single square foot of CIGS deposited on stainless steel and coated with CBD CdS and sputtered ITO at GSE. Ag grids were applied by e-beam. There were 50 small area devices ($0.68cm^2$) per coupon, and all 800 devices were tested. Histograms of V_{oc}, J_{sc}, FF, and efficiency across the sample area are shown in Figure 1.28. The average efficiency of all devices was 8.4%; 79% were between 8% and 11.3%. Although a fraction of the diodes were likely damaged during the diode fabrication process, the areal distribution of device characteristics indicates that the majority of the devices outside the main efficiency distribution were shorted due to defects introduced prior to device fabrication.
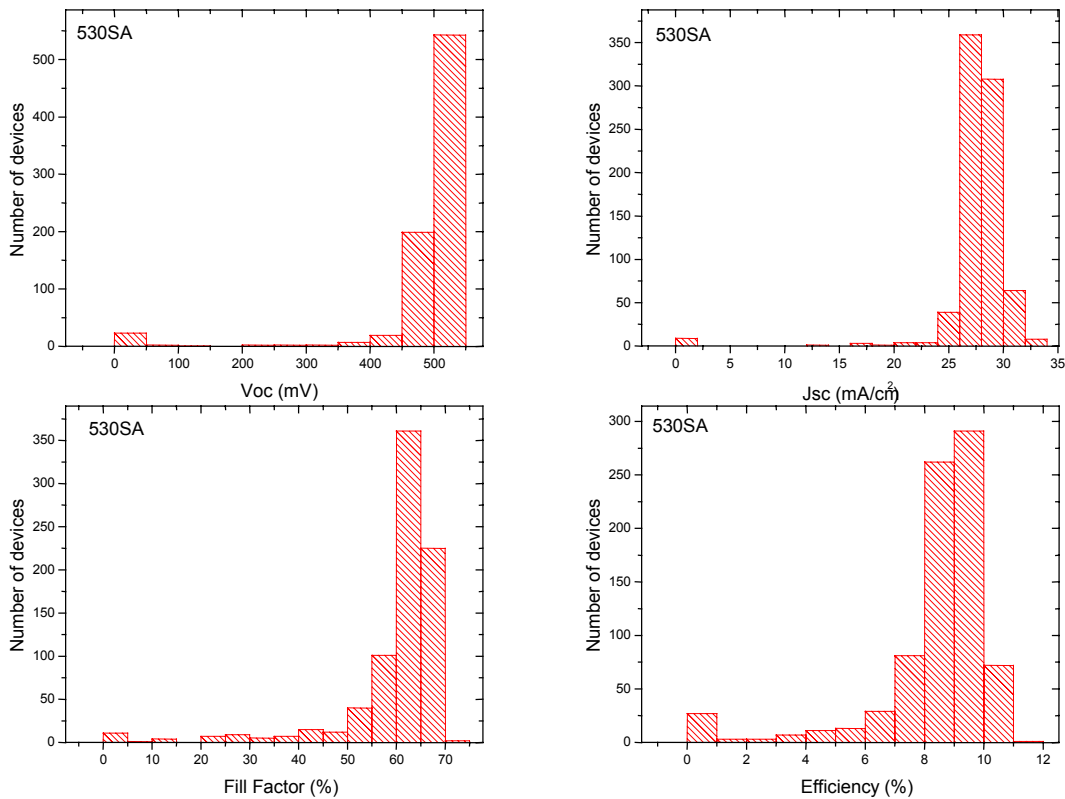

Figure 1.28: Histograms of JV characteristics from devices extracted from a square foot section of web

1.6 Ga Process Control using Atomic Absorption Spectroscopy Flux Measurements

Fundamental mechanisms underlying processing and materials performance relationships in more complex and dynamic thin film structures may not be revealed in post-processing measurements. For these cases, effective feedback process control is critical and underscores the need for real-time measurement and interpretation of system parameters. Although process models and simulators enable development of effective process reactor designs and model-based control strategies, real-time sensing and control of critical process and product variables is required to accommodate unanticipated process upsets, reactor variability/drift, and perhaps allow operation in physically unstable processing regimes where repeatability can be achieved only through dynamic feedback/feed-forward control.

In the present CIGS deposition system, thermocouples provide information about the effusion source temperature, and physical based models provide guidance about expected effusion flux and anticipated film properties. However, sensors must be incorporated in the process path, from the effusion sources to the final thin film product, to provide information that cannot be obtained by other means and to account for unpredictable system dynamics that are not in the process models. The primary controlled parameter is the power supplied to each of the effusion sources. In general, the effusion source temperature and effusion property measurements enable more direct and simple process control. However, due to the large thermal mass of the sources, thermocouple measurements have a very slow response time, limiting the sensitivity and time response for process control. In-situ measurements of the flux are directly related to film thickness and do not have any significant time response limitations, thus providing real-time information about dynamic and unexpected process fluctuations.

Previously, AAS measurements of Cu and In fluxes indicated improved process control compared to thermocouple measurements. However, due to the lower AAS response and lower flux rates of Ga atoms in the CIGS process, additional efforts were performed for this project to design and construct AAS systems to measure Ga flux for in-situ real-time process control. Specifically, as part of a continuous effort to develop and implement sensors for improving intelligent process control of the thin film photovoltaic production, this portion of the Thin Film Partnership Program efforts included:

1) Fabrication, implementation, and evaluation of an improved Atomic Absorption Spectrometer (AAS) head in the CIGS production chamber for monitoring Ga.
2) Development and demonstration of control algorithms for the Ga source effusion rates.

One of the difficult issues for physical vapor deposition (PVD) manufacture of multi-component thin films is the measurement and control of the deposition rate. Conventional quartz crystal monitors are viable in the deposition of single element films, but are insensitive to flux composition and therefore not well suited to the control of multiple effusion sources of varying elements. Ideally, a single in-line flux and chemical identification sensor is desired for the multi-element vapor phase deposition process. This sensor must be able to remotely determine the vapor composition, flux, and flux velocity in real-time – and perhaps also the composition – of the deposited film. Presently, no commercially available or developmental sensor exists that can meet all of these specifications. An atomic absorption spectrometry (AAS) system was identified and procured that provides element-specific optical measurement and control of the

deposition flux. The system relies on AAS principles to measure the vapor phase density of the element of interest. Initial experiments were performed to determine if AAS sensors could be used to monitor the overall effusion rates of copper, gallium and indium by monitoring the absorption in the characteristic spectrum of each species at a representative location in the chamber. The sensors were set up to monitor the absorption in a narrow path across the deposition region. Results of these initial experiments indicated that the AAS system could be used to accurately and reproducibly control copper and indium effusion. However, while Ga flux measurements are theoretically possible with AAS systems for process control four major issues must be addressed:

1) Low flux rates in the GSE CIGS process
2) Relatively low absorption cross-sections
3) Thermal expansion of the optics at the relatively high temperatures near the sources, and
4) Coating of the optics by Ga and an indium selenide species that does not need direct line of sight to deposit on surfaces.

The AAS system allows optical and element-specific measurement and control of deposition flux. Furthermore, since multiple sources of In and Ga are sufficiently separated during processing, AAS measurements will provide independent measurements of the flux and thus film thickness from the individual sources. The system relies on atomic absorption spectroscopy principles to measure the vapor phase density of the element of interest. AAS functions by measuring the attenuation of a beam of light having an element-specific characteristic wavelength. While AAS has been used as a viable wet chemistry measurement for some time, the Atomicas system is the first to apply AAS operation to real-time, element-specific, measurement and control of vapor phase deposition.

The main limitations of the AAS system involve the intensity of the source and detected light and the single element specificity of an individual instrument. These limitations could be overcome with the use of lasers. However, the present cost of a tunable laser or a custom designed laser diode material with the appropriate wavelength is prohibitive for use in an AAS sensor. Furthermore, commercially available diode lasers with the exact wavelength needed for each element do not exist.

For accurate AAS measurements, several conditions must be met including:

The absorption of light must be sufficiently high to match high signal-to-noise ratio
The absorption of the signal must not be too high; otherwise the signal will reach saturation (Figure 1.29)
Proper absorption levels for the AAS system are between ~25 and 50% and can be adjusted by controlling the amount of flux crossing the light path (either by moving to a different part of the plume
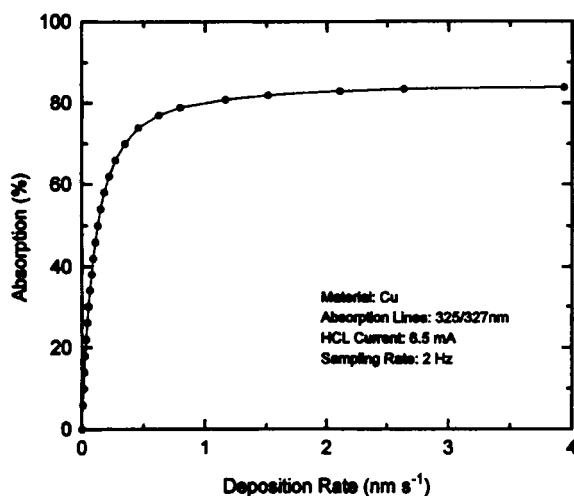

Figure 1.29: Absorption versus deposition rate for Cu

30

where the flux rate is different or by physically blocking part of the flux from crossing the light) Thermal expansion of the optics inside the deposition chamber must not cause significant movement to misalign one or both of the light signals.

Initial dual head AAS systems suffered from limited hardware design that had significant thermal expansion issues at the temperatures used in CIGS processing and that did not adequately keep the optics from being coated by direct line of sight deposition without significant loss of signal throughput. While the AAS system did compensate for an ~10% degradation in signals due to window coating, additional modifications to the base unit were needed to allow for lower signal degradation while maintaining accurate measurements. In addition, a shutter was used to allow for in-situ calibrations while flux is present. A custom optics head was designed and tested to resolve the major issue related to performing AAS measurements in a CIGS deposition system. Furthermore, calculations were performed to identify locations to measure the appropriate Ga flux for optimum AAS signals. Based on these initial designs, a new set of hardware was constructed and tested to measure Ga flux.

For both In and Cu, AAS provided very good control of the measured metal fluxes. The new head design significantly improved signal-to-noise and decreased thermal expansion effects. Thus, due to previous efforts, successful and improved process control have been demonstrated for both In and Cu deposition for CIGS processing.

As discussed above, the initial limitations of the AAS system required a revolutionary new optical head design to transmit and collect the light with absorption from specific fluxes in the very harsh environment of a CIGS deposition system. However, even with the new head design that provided good signal-to-noise of the light sampling the flux, the initial placement of the head to measure Ga flux was not sufficient to provide significant absorption measurements for process

Figure 1.30: Comparison of Ga source temperature and AAS absorption rates of Ga flux in a CIGS chamber with the detection head positioned approximately 2" above and 0.5" to the side of the Ga source. Since a shutter was not available at this point to calibrate the Ga absorption signals, an absolute absorption rate is not known. However, a 15° Celsius change in temperature at nominal deposition temperatures resulted in a 2% absorption change. The absorption falloff is directly related to signal attenuation due to coating on the optical windows.

control in the CIGS chamber. The heads were placed approximately 5-6 inches from the effusion sources. However, due to the relatively small absorption cross-section of Ga and the smaller flux rates measured (as compared to Cu or In), flux absorption measurements for processing conditions were between 0.5 and 1%. Ideally, absorption percentages should be between 30 and 50% for optimum process control signals.

To resolve the low flux issues, the Ga detection head was repositioned approximately 2 inches above and 0.5 inches to the side of the effusion source. The results shown in Figure 1.30 indicate that this new position provided sufficient absorption rates for process control. However, due to the closer proximity to the sources, window coating from an indium-selenium species became even more of an issue. This is an interesting effect that seems to indicate that the In-Se species is formed in the vacuum and creates a situation where coating and low signal issues must be traded against sufficient absorption for process control. Implementation of a shutter to obtain accurate calibrations and improvements in the Atomicas signal processing decreased the effects of these issues.

Initial implementation of PID type control based on Ga Atomicas setpoint measurements was performed and the initial data is shown in Figure 1.31. The data indicates that the AAS system can be used to control Ga flux and thus thickness as well as thermocouples for CIGS production. Algorithm development for control was a relatively straightforward process and, while fine tuning is always required with process changes, the initial work demonstrates that the present process is suitable to accurately use AAS measurements for Ga deposition control.
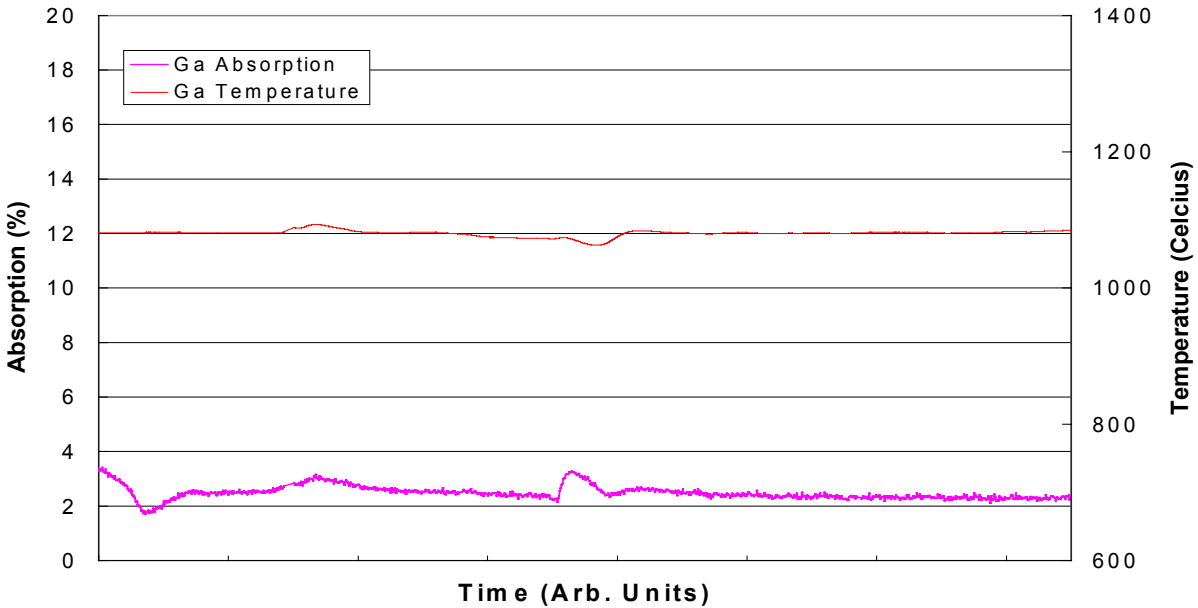
Figure 1.31: Representative absorption measurements of Ga flux under AAS control. The data indicate that AAS can be used to accurately control the Ga deposition for CIGS production.

2.0 MONOLITHIC INTEGRATION OF PV

The objective of this task was to fully develop and optimize scribe and interconnect processes for module formation. Layer-specific, all-laser scribing methods were to be developed, along with ink-jet or screen-printing of conductive/insulating ink patterns. Key issues with development of low-loss scribe and interconnect processes included: meeting requirements for excellent electrical isolation for front and back contact scribes; low series resistance for the interconnect scribe; minimal debris generation, and minimal scribe area loss.

2.1 Layer-Specific Laser Scribing Processes

GSE established optimum scribing parameters for front contact, back contact, and interconnect scribes using all-laser processes. Parameters including pulse repetition rate, pulse power, focus, feed rate, emitted wavelength and spot diameter were varied to achieve selective laser scribing of the front, absorber and back contact layers as required to establish an all-laser process for each of the three scribes. Debris generation and scribe area loss were minimized.

Early in Phase III, improvements in the machine vision aspect of the laser scribing system were made to allow high-resolution inspection of resultant scribes in-situ (with the web still in place on the scribing station). This capability allowed more accurate alignment to minimize scribe spacing. Also, accurate assessment of scribe character was more readily available, as the need to cut samples out of the web and image them remotely was often eliminated. An example of the "in-situ" optical imaging capability is shown in Figure 2.1.

While values of specific interconnect resistivity as low as 0.3 Ω-cm had been obtained, development of process conditions for the interconnect scribe continued. To further minimize the interconnect resistivity and better understand the optimal conditions, testing of the via scribe using special interconnect test patterns was performed. The test patterns were designed to separate resistance contributions due to the front TCO, the influence of the insulating line of ink-jet material covered by TCO and the interconnect itself. However, many of the controlled studies using the ink-jet test pattern were invalidated by the presence of Cu-rich areas of CIGS or by excessively high values of sheet resistivity for the TCO. Highly textured morphology on the CIGS was one possible cause of high sheet resistivity; other conditions for TCO and CIGS deposition were evaluated to minimize this problem.
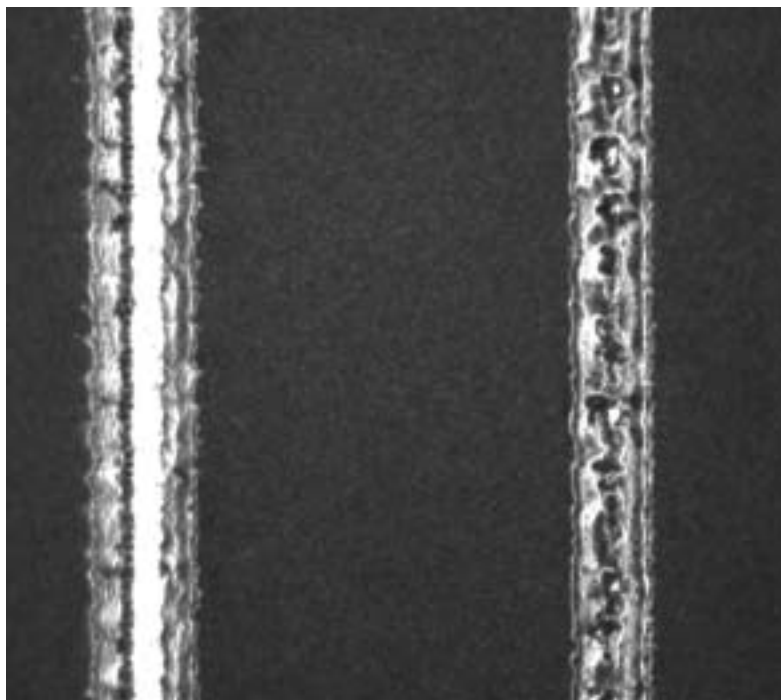

Figure 2.1: An optical micrograph of a back contact and via contact scribe taken on a web during processing with the high-resolution optical imaging equipment on the scribing station

Additional rolls of material with CIGS deposition were selected and processed into interconnect test patterns; the deposited front contact (ITO) ranged in resistivity between 100 and 250 ohms/square. Given such high sheet resistivity, the specific resistivities of the via scribe itself could not be determined reliably. To determine whether CIGS surface morphology was linked to the high sheet resistivity, other CIGS material with a smoother surface morphology was processed through ITO deposition, under identical deposition conditions. Much lower values of sheet resistivity (typically 20 - 30 ohms/square) resulted, confirming that ITO properties are highly dependent on the morphology of the underlying CIGS. As a result, CIGS growth conditions that avoid extremely rough surface morphology are favored.

A major rebuild/re-alignment of all optics and mechanics was accomplished. Several problems were located and eliminated, including laser damage on some optics, accumulated scribing debris on final optics, misalignments and several mechanical problems affecting relative beam separation.

Towards the middle of Phase III, anomalous and variable results were produced that indicated significant current leakage across the front contact scribe. At the same time, radically different scribing power in the beam(s) than that normally used was required to achieve optimized via scribes; this difficulty was suspected to be related to the root causes affecting the front contact scribing. The cause of variability in the scribing process was identified as intermittent malfunction of the laser head. Several failed components inside the laser were replaced by the manufacturer to eliminate the problem. Once the repaired equipment was re-installed and aligned in the system, high quality scribes were produced.

Re-optimization of parameter settings was performed for the via scribe using via test patterns that allow measurement of the specific via resistivity. (Re-optimization was required due to a change in the back contact used on the polyimide substrate.) A first-cut re-optimization was completed on a back contact using alternate materials. Results indicated a fairly broad minima reaching 2 ohm-cm (specific resistivity of the via scribe), although several difficulties, including ink-jet encroachment on the via region, required repetition of the study. Specific resistivities less than 1 ohm-cm are desirable, and had been obtained previously on a back contact of pure Mo.

As program requirements had now been met, no further work was done on the layer-specific laser scribing processes.

2.2 Ink Dispense Technology for Module Integration

GSE designed, fabricated and tested single head ink-dispense methods using ink-jet technology for replacement of screen printing. Process goals were the formation of continuous, uniform ink lines of insulating material having less than 150 μm width and registration accuracy of 50 μm at a speed of 22 cm/sec. If insurmountable difficulties were encountered, GSE was going to optimize the screen printing techniques that were already in use for line printing on module interconnects.

Commercial sources were identified who were capable of fabricating extremely small and precise components needed for the ink-jet dispense heads, and new designs were evaluated for the ink-jet dispense tip, to further minimize linewidth of the printed insulator over the back contact scribe. Registration accuracy between the printed ink-jet line, the back contact scribe and the interconnect scribe made during the first laser operation continued to be excellent, despite several changes to the system that increased speed and throughput.

As Phase III continued, the ink-jet line width remained the dominant factor in total scribe interconnect width, and thus dead area loss. Although ink-jet printed lines approaching 100 μm in width were printed, routine setup and operation still resulted in lines that were typically about 250 μm wide. Suppliers for ink-jet dispense tips having smaller orifice diameters were located and the tips were procured. The receiving mounts and the suspension for the ink-jet tips were modified and tested; the new suspension appeared to work well, though the beginning and end of the ink-jet deposition was often marked by a greater deposited ink volume. As increased ink deposition near the module edges could be a problem in processing long rolls of material, because of the cumulative effect on rolled web diameter, efforts were made to eliminate the problem.

When problems with frequent clogging and reproducibility were encountered with the smaller orifice diameter dispense tips, a series of systematic experiments was conducted to identify the cause of the clogging and skipping. As a result of changes in the dispense tips and measures taken to prevent solidification of ink on the dispense tips, the problems with frequent clogging and consistency of the ink-jet deposition were largely eliminated.

Problems also arose in the ink dispense operation when there was a changeover to a new batch of fluid whose shelf life was approaching. These problems arose because ink viscosity increases substantially with time over a span of four months. Partial compensation for the viscosity changes was achieved by changing both the orifice size in the dispense tips and the dispense parameter settings.

With these final modifications, program requirements for this subtask were met, and attention was shifted elsewhere.

2.3 Process Optimization to Reduce Scribe Area Loss

GSE's goal was to minimize printed line widths, scribe widths and registration tolerances and compress total scribe area width progressively from 625 μm to less than 300 μm to maximize module efficiency. GSE also was to determine optimum module segment width for high efficiency module fabrication.

To compress the total scribe interconnect width to 300 μm or less, reductions were needed in the ink-jet printed line width. Although excellent registration between ink-jet printing and laser cutting in a single beam, single ink-jet mode had been demonstrated, improvements were needed in registration accuracy between ink-jet depositions and laser cuts in the multiple beam/ink-jet process then being used. Errors in beam separation reproducibility and control were traced to

mechanical components (fine pitch lead screws having faulty couplings and shaft misalignment); replacement parts were installed to eliminate the problem. Once these parts were installed, scribe placement errors were significantly reduced.

As Phase III continued, systematic efforts were made to reduce total scribe interconnect and printed ink line widths – and results were achieved that met the final goal of 300 μm for total interconnect width originally set out in the Thin Film Partnership Program. Figure 2.2 shows a micrograph of the all-laser and ink-jet interconnect that is about 260 μm total in width.

Further effort was directed toward making the 250-300 micron total interconnect widths on a continual basis in spite of variations in substrate and process parameters.
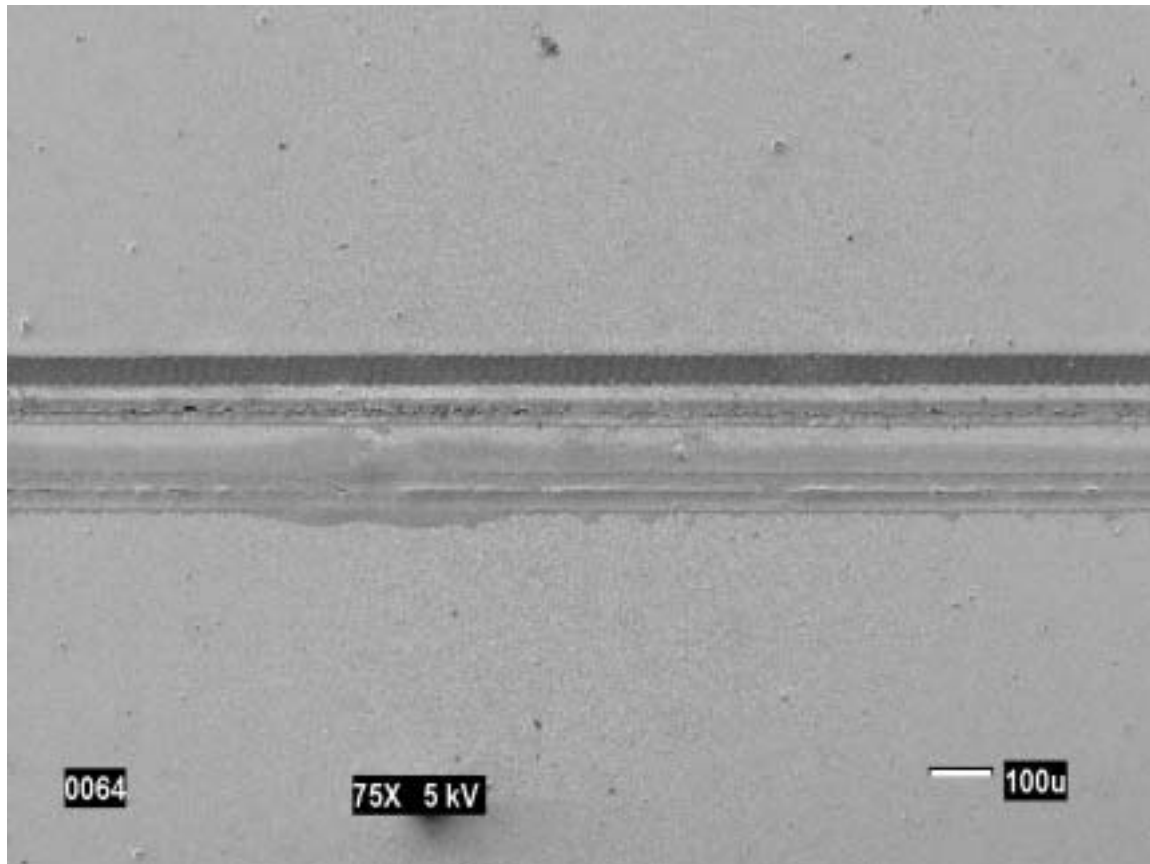
Figure 2.2: An SEM micrograph of a monolithic interconnect made with the process developed at GSE. The total interconnect width is about 260 μm, showing (top to bottom) the front contact scribe, the via scribe and the back contact scribe/ink-jet printed insulator.

2.4 Process Scaling

GSE demonstrated roll-to-roll scribing on 33 cm × 300 meter rolls. Scribe and ink line printing parameters were optimized initially using module test patterns, then submodules and, finally, modules.

As the program proceeded, submodule development began with fabrication and measurement of submodules up to 200 cm^2 and emphasis progressively shifted to module fabrication on larger areas. During Phase III, a significant number of 32-in. $\times$ 11.5-in. (2370 cm^2) modules were fabricated using CIGS on polyimide. These represented the largest, monolithically integrated modules patterned at GSE to date. The module fabrication worked well, except for an apparent shift in the segment width between the first and second laser operations, which resulted in a cumulative registration error. The cause of the shift appeared to be due to a small differential stretch in the web between the two laser operations, related to web tensioning. Provisions were implemented to correct "on the fly" for any change in web dimension.

In addition, module patterns were made for 12-in $\times$ 30-in modules with 3 mm wide segments. Successful patterning of test material produced modules having output voltages of 50 to 75 volts when cut into sections that were 2-in $\times$ 30-in. Problems encountered were shunting, high series resistance and CIGS material of low quality; efforts were made to address each of these issues.

Progress achieved in producing 50 to 75 volt output in subpanels for high voltage modules was extended, as full modules in a 12-in $\times$ 30-in format were produced. Each module incorporated almost 1300 monolithic interconnects over an aperture area of 2000 cm^2. Under outdoor conditions the modules produced over 500 volts (open circuit); the best one having 585 volts V_{oc}. Preliminary data indicated that the output voltage was equal to or, in some cases, exceeded that expected based on the average V_{oc} of matrices of devices made adjacent to the modules on the web, as shown in Figure 2.3.
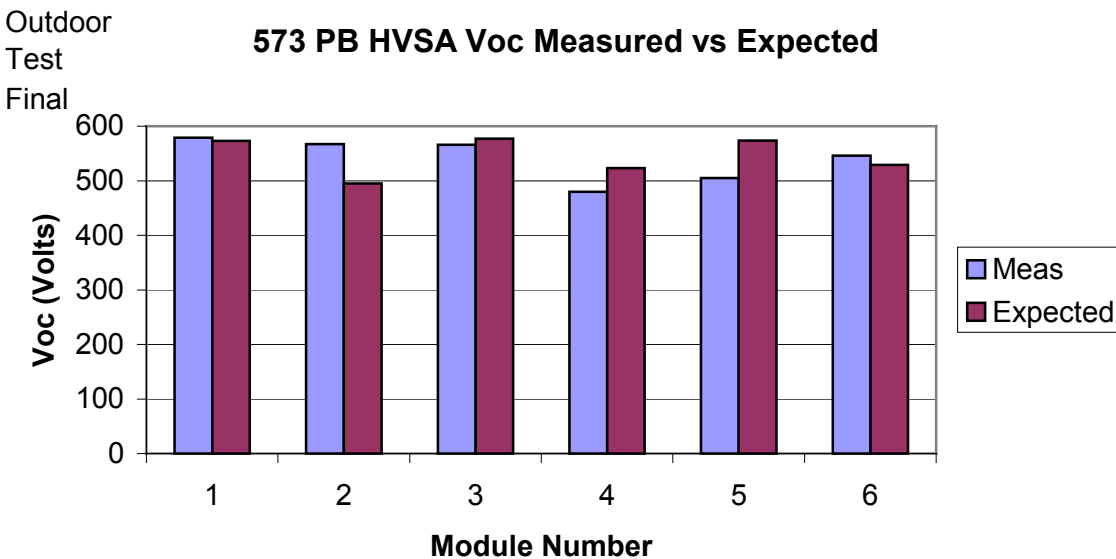
Figure 2.3: **The measured open circuit module voltage compared to that expected based on small area devices near the module on the web**

3.0 ENCAPSULATION DEVELOPMENT AND RELIABILITY TESTING

The objective of this task was to begin development of viable encapsulation and finishing methods to produce flexible and rigid mounted PV products. Key issues with this task were the development of front and back sheet materials, methods for lamination, and buss and power output connections.

GSE Product Description

GSE developed four product lines comprised of cells or modules envisioned to meet the needs of the initial markets identified. The goals of this NREL subcontract allowed focused efforts to be applied to developing and demonstrating first generation product designs. The four primary products follow:

1. **Unlaminated Submodules:** For product lamination and finishing via strategic, specialty partners (see Figure 3.1 for a roofing shingle that utilizes GSE submodules).
2. **Portable Power Pack's™:** Foldable, flexible modules with reinforced nylon backing (Figure 3.2).
3. **Power Flex™:** Foldable, flexible power modules with reinforced nylon backing.
4. **Power Flex™ Semi-Flexible:** Power modules with aluminum backing to be UL listed.
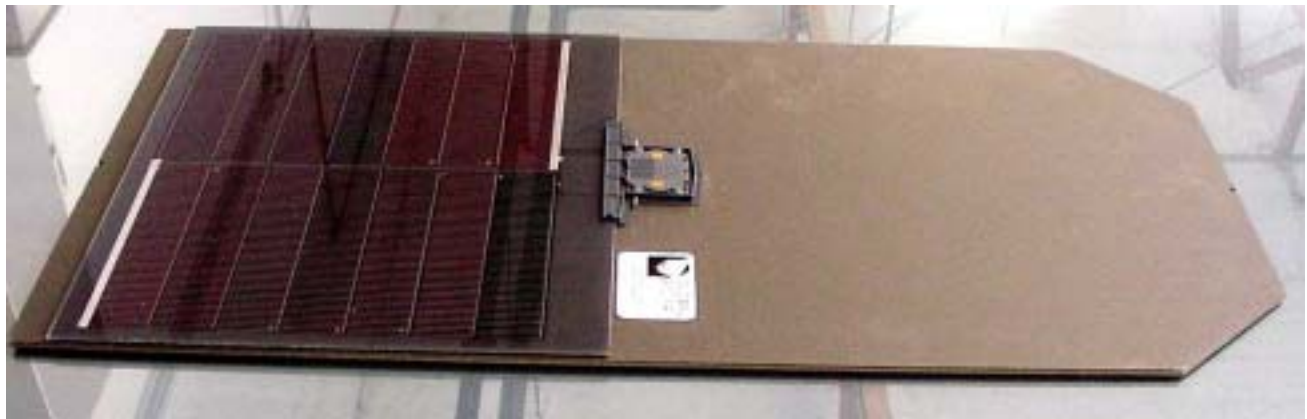
Figure 3.1: Roofing shingle incorporating GSE's photovoltaic submodules

Figure 3.2: GSE's Portable Power Pack™

Overall Progress

During Phase III, the focus within the Encapsulation Development and Reliability Testing Task was directed toward demonstration and initial pre-certification of various product designs developed for selected GSE market sectors. Considerable product development occurred and feedback from customers was extremely helpful. Both flexible and semi-flexible backed products were developed based on a structure of Tefzel - EVA - Thin module - EVA - selected backing material (depending on the product line).

During this time, GSE prepared for a demonstration of the Power Flex™ product line as part of a Transportable AC System (TACS) for use by the military. A photo of the application is shown in Figure 3.3. Note that each sub-array is made up of 14 modules each measuring ~26-in. × ~55-in. The power sources are on the trailers.

Figure 3.3: Power Flex™ modules on ground

GSE also prepared for a demonstration of the Power Flex™ product line attached to the fly on a general personnel tent utilized by the military. The demonstration took place at AFRL at Ft. Tyndall, FL. A photo of the application is shown in Figure 3.4. The modules are attached to the fly of the tent and the array is designed to charge the battery bank of a Transportable AC System (TACS), similar in nature to the power center shown on the right trailer in Figure 3.3.

Figure 3.4: Power Flex™ modules on tent during tent deployment

In the following quarters, primary efforts were redirected toward initial pre-certification of selected product designs and product reliability testing, toward the goal of product certification.

3.1 High Speed Lamination

GSE designed, assembled and evaluated methods and equipment for high-speed lamination of front and back sheet onto CIGS PV in a flexible product. The objective of this subtask was to design, fabricate, install, and test lamination equipment capable of low-cost lamination of solar panels that met initial throughput, economic, and market needs of GSE. GSE also evaluated the use of adhesives to replace EVA.

As a result of early efforts and experience with prototype equipment, equipment to meet the initial lamination goal rate of ~1ft^2 per minute was standardized, thereby fulfilling program requirements.

3.2 Lamination of Flexible Substrate to Low Cost Rigid Backing

GSE evaluated methods for incorporating CIGS on flexible substrates into a rigid mounted product. GSE also surveyed and conducted preliminary suitability tests on possible back and front sheet materials and adhesives, including pressure sensitive adhesives.

Two primary areas were focused on initially in the area of low-cost rigid substrates. The first was development of roof shingles comprised of GSE submodules laminated onto slate substrates (Figure 3.5). Prototypes were demonstrated and, when efficiency goals were achieved, certification efforts proceeded.

The second key focus was development of modules formed on a thin aluminum backing. The primary structure used was Tefzel – EVA – SS PV substrate –- EVA – aluminum sheet. This structure passed structural loading tests and lead attachment load tests. The inclusion of a barrier film interlayer and cell barrier coatings were investigated as ways to reduce the ingress of water and oxygen and thereby increase module reliability. Films that underwent trials for use as an interlayer included PET, PVDC, BOPP, and other OPP barrier materials. To further improve the reliability of the final module, direct coatings onto the cell and possibly onto submodule assemblies of cells were investigated by comparing the rates of corrosion of cell structures in modules with and without the additional barrier film interlayer. Vapor deposition type coatings such as Parylene and easier-to-apply UV curable acrylics, acrylic-urethanes, and sprayable air dry acrylics also underwent trials that compared the rates of cell structure corrosion in modules with and without the coatings.

3.3 Power Lead and Buss Attachment

GSE designed and evaluated processes for attachment of metallic buss and power leads to flexible and rigid CIGS PV products. The objective of this subtask was to design, demonstrate, and incorporate parts, materials, and procedures for the range of steps in solar module fabrication from buss bar application to power lead attachment in order to meet initial throughput, economic, and market needs of GSE.

The reinforced nylon backed modules (**Portable Power Pack™** and **Power Flex™)** utilize stitched stress relief areas and no junction boxes on the module. Incorporation of a bypass diode or a blocking diode, as desired, into the module structure rather than in the cable was evaluated. A defined wire specification and appropriate stress relief (in the case of the flexible modules) resulted in easily passing the UL power lead Strain Relief Test.

Early in Phase III, each of the products described in the GSE Product Description section of this report was relatively well defined in the power lead and buss attachment areas; little additional effort was required.

3.4 Module Performance and Reliability Testing

The goal of this subtask was to develop tests and equipment for measurement of module efficiency and reliability. Basic module test equipment, including large area solar simulators for JV measurement and equipment for wet hi-pot testing was set up. An outdoor test site at the GSE Tucson facility also was set up for long-term evaluation of module output and durability. Initial tests for wet hi-pot, mechanical load, thermal cycling, humidity cycling, and impact were carried out both at GSE and at external facilities.

Though passing UL and other certification tests is paramount to success in the PV roofing and building market, GSE determined in the early quarters of Phase III that feedback from the demonstrations of initial products was of more value at that time than the actual UL certifications. As a result, virtually all product development efforts initially went into product demonstration, identification of improvements, and upgrade of designs for further testing. This effort resulted in product designs that were expected to meet and exceed initial market requirements. Focus during later quarters was on further demonstration, stress testing, and certification of aluminum-backed Power Flex™ semi-flexible modules.

Additional personnel to support reliability efforts were added, along with additional electrical and mechanical test equipment for in-house testing and improvement of modules. Environmental test chambers, a peel tester, a hi-pot tester, a scratch tester, a push tester, an impact tester, and a mechanical load tester were ordered or available for testing. Procedures for in-house testing per UL, IEEE, and IEC standards were written and used for development of the modules prior to submission to the UL Laboratory. To ensure success, both in-house and UL Laboratory testing per UL, IEEE, and IEC standards for screening and evaluation of module efficiency and reliability were performed prior to executing product certification testing. For developmental testing, the UL Laboratory, also known as ASU-PTL East, was used for long-term testing and other types of tests that could not be done in-house. Mechanical load tests simulating wind loads and mechanical pull tests on electrical cables and junction boxes were successfully passed in-house.   As the module design progressed through different stages, developmental tests for each stage were completed.

Once the preliminary design of the aluminum-backed module (semi-flexible) expected to pass UL was completed, GSE began gross in-house testing. The preliminary upgraded design version of the Portable Power Pack (P3) module (flexible) also was identified and gross in-house testing performed.

Later, GSE locked-in a design and all materials for the aluminum-backed module (semi-flexible) expected to pass UL, completed prototypes of the semi-flexible module with all standard components and processing, and submitted prototypes and test structures of both the semi-flexible and flexible modules for evaluation through UL-type tests at ASU.

Throughout the tests on the semi-flexible prototype, only two failures were observed:
The J-Box adhesive failed (recommended alternatives were evaluated prior to resubmitting).
The quality of Tefzel grade led to some visible failures (alternative grades were evaluated and quality efforts were made with the supplier).

Near the end of Phase III, the fire test was the only design-affecting test still to be accomplished on the standard semi-flexible module design. Testing continued through the remainder of Phase III. Humidity cycling revealed periodic module failure due to an as-yet unexplained corrosion problem; further work is required to identify and eliminate the issue.

Summary

During the third and final year of effort under this subcontract, a number of significant advancements were made. Robust effusion sources with good uniformity and reproducible characteristics along with insights useful for future design improvements were demonstrated. Once specific engineering issues related to thermal expansion, optical coating, and baseline drift were properly addressed, the AAS system successfully provided good and reproducible Ga (also Cu and In) flux measurements for CIGS production. Furthermore, the use of standard control algorithms to provide setpoints in a closed-loop multiple level controller was sufficient to demonstrate the utility of AAS to provide Ga thickness control during CIGS deposition.

The CIGS process development based on Design of Experiment techniques was successful in revealing process sensitivities and parameters that required adjustment for optimized efficiency. The evaluation of various stainless steels enabled selection of the most suitable substrate type to maximize efficiency. Improvements in the uniformity and control of Na delivery in conjunction with the optimization of Na concentration for efficiency were also made. As a result of re-baselining the CIGS deposition process, small area test cells with efficiency exceeding 12% and production cells with efficiency greater than 10% were demonstrated, using the production equipment.

Scribe processes were successfully developed that minimized leakage currents and impedance losses. Ink-jet processes were developed that met the program goals for linewidth, registration accuracy, and print speed. In tandem, the laser-scribing and ink jet processes were demonstrated on 33cm × 300m rolls and found capable of achieving scribe area losses of less than 300 µm. Additional work is required to make the interconnect processes more robust to variations in substrate and process parameters.

A number of methods for incorporating CIGS on flexible substrates into both flexible and rigid products were investigated. Successful techniques for power lead, buss attachment, and high speed lamination were developed. Many configurations were tested for reliability by wet hi-pot, mechanical load, thermal cycling, humidity cycling, and impact at GSE and external facilities to arrive at an optimized configuration for both product types.

Acknowledgements

Global Solar Energy wishes to acknowledge the contributions of the following people and organizations:

REPORT DOCUMENTATION PAGE

Public reporting burden for this collection of information is estimated to average 1 hour per response, including the time for reviewing instructions, searching existing data sources, gathering and maintaining the data needed, and completing and reviewing the collection of information. Send comments regarding this burden estimate or any other aspect of this collection of information, including suggestions for reducing this burden, to Washington Headquarters Services, Directorate for Information Operations and Reports, 1215 Jefferson Davis Highway, Suite 1204, Arlington, VA 22202-4302, and to the Office of Management and Budget, Paperwork Reduction Project (0704-0188), Washington, DC 20503.

1. AGENCY USE ONLY (Leave blank)	2. REPORT DATE April 2003	3. REPORT TYPE AND DATES COVERED Final Technical Report 5 February 1998–4 February 2001

4. TITLE AND SUBTITLE
Process Development for CIGS Based Thin Film Photovoltaic Modules, Final Technical Report, 5 February 1998–4 February 2001

6. AUTHOR(S)
J. Britt, S. Wiedeman, M. Beck, and S. Albright

5. FUNDING NUMBERS
PVP35001
ZAK-8-17619-04

7. PERFORMING ORGANIZATION NAME(S) AND ADDRESS(ES)
Global Solar Energy, Inc.
5575 South Houghton Road
Tucson, Arizona 85747

8. PERFORMING ORGANIZATION REPORT NUMBER

9. SPONSORING/MONITORING AGENCY NAME(S) AND ADDRESS(ES)
National Renewable Energy Laboratory
1617 Cole Blvd.
Golden, CO 80401-3393

10. SPONSORING/MONITORING AGENCY REPORT NUMBER
NREL/SR-520-33651

11. SUPPLEMENTARY NOTES
NREL Technical Monitor: H.S. Ullal

12a. DISTRIBUTION/AVAILABILITY STATEMENT
National Technical Information Service
U.S. Department of Commerce
5285 Port Royal Road
Springfield, VA 22161

12b. DISTRIBUTION CODE

13. ABSTRACT *(Maximum 200 words)*: Global Solar Energy initiated an extensive and systematic plan to accelerate the commercialization of thin-film photovoltaics (PV) based on copper indium gallium diselenide (CIGS). The distinguishing feature of the GSE manufacturing process is the exclusive use of lightweight, flexible substrates. GSE developed the technology to fabricate CIGS photovoltaics on both stainless-steel and polymer substrates; over the course of the Thin Film PV Partnership program, however, stainless steel showed significant advantages. CIGS deposited on flexible substrates can be fabricated into either flexible or rigid modules. Low-cost, rigid PV panels for remote power, bulk/utility, telecommunication, and rooftop applications have been produced by affixing the flexible substrate to an inexpensive rigid panel by lamination or adhesive. There have been numerous challenges in developing the technology for manufacturing flexible CIGS photovoltaic modules. Three major areas deemed exceptionally challenging were selected by GSE for focused development under the Thin Film PV Partnership Program: 1) CIGS absorber improvement, 2) monolithic integration, and 3) encapsulation. Most conventional techniques for monolithic integration of thin film PV devices on glass substrates cannot be applied to integrate devices on a polyimide substrate. Novel interconnect schemes and processes had to be developed. The encapsulation of a flexible module also presented special problems to solve, and unique advantages to employ.

14. SUBJECT TERMS: PV; CIGS absorber; deposition process optimization; heterojunction; process scaling; atomic absorption spectroscopy (AAS); monolithic; laser scribing; high-speed lamination; thermal cycling;

15. NUMBER OF PAGES

16. PRICE CODE

17. SECURITY CLASSIFICATION OF REPORT Unclassified	18. SECURITY CLASSIFICATION OF THIS PAGE Unclassified	19. SECURITY CLASSIFICATION OF ABSTRACT Unclassified	20. LIMITATION OF ABSTRACT UL